SHAKEDOWN CHARACTERIZATION OF AN INSTRUMENT FOR NANOCUTTING AND NANOINDENTING

By

MATTHEW JOSEPH KLOPFSTEIN

Bachelor of Science
The Ohio State University
Columbus, Ohio
1991

Master of Arts
The Ohio State University
Columbus, Ohio
1992

Submitted to the Faculty of the
Graduate College of the
Oklahoma State University
in partial fulfillment of
the requirements for
the Degree of
MASTER OF SCIENCE
December, 1997

OKLAHOMA STATE UNIVERSITY

SHAKEDOWN CHARACTERIZATION OF AN INSTRUMENT FOR NANOCUTTING AND NANOINDENTING

Thesis Approved:

Don A. Lucca

Thesis Adviser

Ronald L. Dougherty

Wayne B Powell

Dean of the Graduate College

ACKNOWLEDGEMENTS

I would like to thank my adviser, Dr. Don A. Lucca for his encouragement, patience, guidance and assistance. I would also like to thank my committee members, Dr. Ronald L. Dougherty and Dr. Eduardo A. Misawa for their valuable comments and suggestions.

The financial support of the Division of Design, Manufacture and Industrial Innovation of the National Science Foundation, and the Oklahoma Center for the Advancement of Science and Technology is gratefully acknowledged. I would like to thank Mr. Gene Cantwell of Eagle-Picher Research Laboratory for his assistance and support.

I would like to thank my colleagues, Mr. Kim-Cheng Tan, Dr. Yin Ming Wang, and Mr. Pai Chou for all their help and valuable suggestions.

Finally, I would like to thank my parents for their continuing support and encouragement.

TABLE OF CONTENTS

LIST OF TABLES

LIST OF FIGURES

Chapter 1

Introduction

The process of mechanical material removal is not well understood at depths of cut of less than a micron or so. Especially of interest is the removal mechanism for brittle materials at this length scale. Commercial instruments have been used to investigate material removal but are limited at small depths of cut (less than 30 nm) in part because of the asynchronous motion of the spindle and the ability to measure forces.

The University of North Carolina at Charlotte and Oklahoma State University have collaborated to design, build and test an instrument capable of investigating the mechanics of nanometric material removal. The first prototype instrument was designed and built at the University of North Carolina at Charlotte(UNCC). Whereas the initial design and construction was performed at UNCC, this thesis describes subsequent refinements and shakedown testing required to make the instrument operational. Originally, the instrument was designed to perform cutting experiments but during the latter stages of development its potential to perform indenting was also recognized.

Chapter 2 is an overview of the design process and the final design of the instrument. Chapter 3 presents the modifications that were made to the original design of the instrument. Chapter 4 details the calibrations that were done before the experiments were performed. Chapter 5 then presents the experimental procedure used.

Chapter 6 explains the analysis of the data and discusses the results. Chapter 7 is the summary and presents areas for future work.

Chapter 2

Instrument Design

2.1 Conceptual Design and Initial Specifications

2.1.1 Conceptual Design

The design and initial construction of the instrument was performed at the University of North Carolina at Charlotte and is reported in detail elsewhere [1]. This chapter serves as a summary of the design and an introduction to the instrument. The instrument was designed to investigate material removal processes at the submicrometer scale. In particular, the capability for cutting at depths of cut below 30 nm was targeted because commercial diamond turning machines are limited in this range. Although not initially conceived as an instrument which could perform "nanoindentation", during the evolution of the shakedown testing, the instrument's potential capability for indentation was also recognized.

Figure 2-1 is a schematic representation of the cutting geometry. The sample is mounted on a piezoelectric tube and the tool is held stationary. The piezoelectric tube provides displacement in three orthogonal directions. Computational and experimental results on these tubes show that a practical lateral cutting range of ± 5.5 μm, with a depth of cut variation of 3 μm is achievable [2]. Of this 3 μm, 1 μm will

be used for fine-positioning of the sample near the tool and 2 μm will be the range for the depth of cut. Mounted on the tool are two force transducers to measure the cutting and thrust force. The cutting direction is along the X axis, as shown in Fig. 2-1.

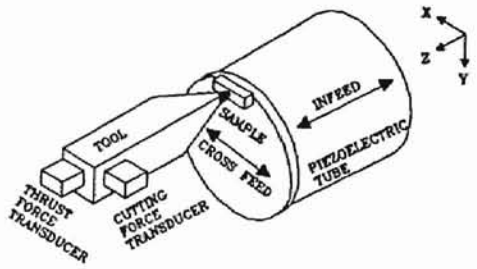

Figure 2-1: Conceptual design of the cutting geometry (from [1]).

2.1.2 Positioning System

The positioning system is composed of two parts: coarse-positioning and fine-positioning. The coarse-positioning system is used to move the sample near the tool, with the gap between the sample and tool being less than the range of motion of the fine-positioning system. The fine-positioning system is used to position the sample so that it just makes contact with the tool without damaging the sample or the tool and to perform the cutting action. The main factors influencing the selection of the coarse-positioning system are repeatability, stiffness and compactness. The required range for this system is about 10 mm which is the space required to kinematically mount the sample on the piezoelectric tube. A linear slide in which the slide moves along guideways was chosen over a flexure slide in which the slide is held by a flexural spring because of the range and stiffness required. The main factors influencing the selection of the fine positioning system are resolution, stiffness and compactness.

A piezoelectric element was chosen because of its resolution and stiffness. A piezoelectric tube rather than a stick-type piezoelectric element was used because of the reduced cross coupling and higher resonant frequency of the piezoelectric tube. The piezoelectric tube must have a resonant frequency that is high enough so that the tube scanner-system is not excited by the cutting action.

The sample-tool contact is accomplished by oscillating the sample at some suitable frequency and monitoring the output of the thrust force transducer with a lock-in amplifier as the sample is moved closer to the tool. The force transducer output signal will correspond to the frequency of the piezoelectric tube when the sample comes in contact with the tool. To avoid damaging the sample or tool, the oscillation amplitude of the piezoelectric tube should be small and the sample should move in small steps toward the tool. The system design allows nanometer scale amplitudes and step sizes to be used.

2.1.3 Force Measurement

Measurement of forces in the X and Z directions (cutting and thrust force) can be made with either a two component force dynamometer or two single-component force dynamometers. Estimates of the thrust force and cutting force are based on previous ultraprecision machining studies[3]. In Te-Cu, the thrust force per unit width at a depth of cut of 2 μm was about 4 N/mm and the cutting force at the same depth of cut was found to be about 6 N/mm[3]. To obtain an estimate for the forces at very small depths of cut, the data was extrapolated to a depth of 1 nm. The forces were found to level off at about 20 nm. The estimate for the cutting force per unit width at a depth of cut of 1 nm, again in Te-Cu, was 83 mN/mm and 63 mN/mm for the thrust force per unit width[3]. For a sample width of 200 μm the smallest force expected is 12 mN. The initial specifications for the force transducers are given in Table 2.1

A force dynamometer with two orthogonal single-axis flexures in a single block of

Resolution	1 mN
Range	0-2 N
Stiffness	At least 25 MN/m
Frequency Response	At least 4 kHz

Table 2.1: Initial specifications for the force transducers

metal was considered. The motion of the flexure would be measured by a capacitance gage to measure the torque applied to the flexure. It was calculated that by using either aluminum, steel or beryllium copper for the dynamometer the design stiffness could not be met. Two piezoelectric force transducers were chosen because they met the design specifications[4].

2.1.4 In-feed Measurement

The in-feed displacement transducer should have nanometer resolution. The transducer will be mounted inside the piezoelectric tube. A linear variable differential transducer (LVDT) and a capacitance gage were considered. It was found that the LVDT was not suitable because of heat dissipation in the piezoelectric tube.

2.2 Implemented Design

The design which was chosen to implement the concept is described below. The instrument has two modules, shown in Fig. 2-2, the force tripod and the horizontal slide. The force tripod houses the tool holder and the force transducers. The horizontal slide houses the piezoelectric tube and the sample mount holder. The function of the horizontal slide is to position the sample near the tool. The overall dimensions of the instrument are 7.5 in. by 5 in. by 2.5 in. high.

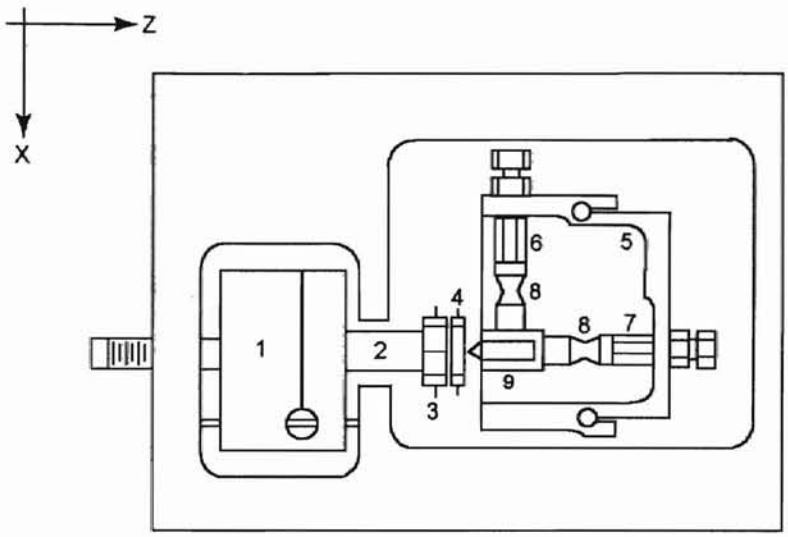

1 Horizontal Slide
2 Piezoelectric Tube and Cap Gage
3 Sample Mount Holder
4 Sample Mount
5 Force Tripod
6 Cutting Force Transducer
7 Thrust Force Transducer
8 Dual-axis Flexures
9 Tool and Tool Holder

Figure 2-2: Schematic diagram of Nanocut.

Resolution	0.2 mN
Range	9.786 N
Stiffness	350 MN/m
Frequency Response	300 kHz

Table 2.2: Specifications for the force transducers used in the instrument

2.2.1 Force Tripod

Two single-component piezoelectric force transducers are used. The relevant specifications for the transducers (PCB Piezotronics KL209A) are shown in the Table 2.2 [4]. The preload on the transducers is adjusted by a preload screw and held in place by a locking nut. The amount of preload applied to the transducers was not initially specified but was later adjusted as outlined in Chapter 4.

The tool is held in the tool holder by two set screws. The tool holder is supported at the bottom by a dual-axis flexure. Dual-axis flexures (8 in Fig. 2-2) are between

the tool holder and the force transducers also. These two dual-axis flexures are used to de-couple the measured cutting and thrust forces. The dual-axis flexures de-couple the forces since they are designed to be two orders of magnitude stiffer in the axial direction than in the flexural (off-axis) directions.

The force tripod has to be designed to have a sufficiently high mechanical natural frequency to prevent resonance when measuring short duration forces. A generally accepted criterion is that the natural period of vibration of the transducer should be smaller than one-third of the shortest pulse occurring during the force measurement[5]. If one assumes a maximum cutting speed of 0.3 m/min and a cutting length of 10 μm, the shortest duration pulse for this application is 2 msec. Thus the force tripod should have a natural frequency of at least 1.5 kHz. The force tripod was designed to have a natural frequency of 2.5 kHz by consideration of the flexural stiffness of the dual-axis flexures.

The axial stiffness of the dual-axis flexures was designed to be 3×10^7 N/m which is close to the stiffness of the piezoelectric tube. The upper limit of the flexural stiffness is determined by the amount of decoupling between the thrust and cutting force that is required; the lower limit is determined by the natural frequency requirement. The flexural stiffness was designed to be 3×10^5 N/m. The stiffness of the dual-axis flexures was estimated by the Paros and Weisbord method[6] and a finite element analysis was performed [1].

The force tripod was designed to move vertically by the positioning of an adjustment screw. The force tripod slides vertically on two precision shafts. The guideways in the force tripod are made to match the precision shafts by using a replicating agent[7].

The force transducers were initially calibrated using deadweights over the range 9.8-490 mN. The force tripod was put in a fixture such that the deadweight applied a compressive force to either the thrust or cutting transducer. When the weight was removed, the voltage change was recorded with an oscilloscope. At each load the

deadweight was removed 2 times. The transducers have since been recalibrated using the method explained in Chapter 4.

An estimate of the cross coupling between the two force transducers was made by unloading one transducer and monitoring the output from both transducers. There was no detectable cross coupling when a force was applied to the thrust force transducer. Cross coupling between the transducers was observed when a force was applied to the cutting force transducer however. This is thought to be because of the torsion experienced by the dual-axis flexure supporting the tool holder and preloading the two force transducers. Originally the cross coupling between the cutting and thrust force was measured to be 11%, more recent measurements indicate a value less than 5%.

2.2.2 Horizontal Slide

Coarse-positioning System

The horizontal slide has a coarse-positioning range of 7 mm. The slide is driven by an 80 thread per inch (TPI) screw. The horizontal slide is mounted onto the structure with one side of the slide having Delrin® bearings and sliding over a precision shaft; the other side is supported on a ball that slides on a flat.

Fine-positioning System

A piezoelectric tube scanner is used as the fine-positioning system. The piezoelectric tube is made of lead zirconate titanate (PZT) and is 25.4 mm long and about 12 mm in diameter. The piezoelectric tube can be moved in three orthogonal directions by the application of a suitable voltage. The piezoelectric tube is divided into four quadrants. To move in either lateral direction, a voltage is applied to two opposite quadrants. To move longitudinally, a voltage is applied to all four quadrants. The sample is kinematically mounted to the front of the piezoelectric tube. The X and Y

axes have a sensitivity of 28 nm/V and the Z axis has a sensitivity of 8 nm/V. The functions of the fine-positioning system are to establish a reference for the depth of cut and to perform the cutting action. The cutting action is achieved by controlling the voltage applied to the X and Z electrodes of the piezoelectric tube (the cut is made in the X direction).

To establish the sample-tool contact, the sample is oscillated at a user determined frequency and advanced toward the tool. The frequency was initially determined by exciting the force tripod with a loudspeaker at various frequencies and monitoring the thrust force output. The thrust force transducer output was observed to have a predominant spike at 236 Hz, thus this was the frequency at which the sample is oscillated. Subsequent measurements, to be discussed in Chapter 4, have cast doubt on this technique for determining the appropriate frequency to oscillate the sample. This same frequency (236 Hz) was used as the reference signal for the lock-in amplifier. When the sample contacts the tool, the output of the thrust force transducer will vary sinusoidally with a frequency of 236 Hz. To prevent any damage to the sample the amplitude of oscillation should be as small as possible. Initially it was thought that an amplitude of oscillation of about 1 nm could be achieved, but this failed to take into consideration the effect of the piezoelectric transducer tube amplifier. Initially then the amplitude of oscillation of the piezoelectric tube was about 20 nm. Subsequent experiments as described in Chapter 5, use an oscillation of about 15 nm. This value is limited by the lock-in amplifier that is currently used because it can not use a signal with a smaller voltage as the reference signal. Initially the sample was pulled back from the tool by 50 nm once the lock-in amplifier senses an output voltage from the thrust force transducer. The pull back distance has since been increased to 75 nm because of the less stable thermal environment currently available at OSU.

2.2.3 Sample mount

The sample is kinematically mounted to the piezoelectric tube by using a Maxwell (3 Vee) coupling. The sample mounting system consists of a sample mount and a sample mount holder. The sample mount holder is the base of the Maxwell coupling consisting of three gothic arches positioned 120° apart. The sample mount holder is glued with a two part epoxy on the front end of the piezoelectric tube. The sample mount has three balls positioned 120° apart which seat into the gothic arches in the sample mount holder. Initially the sample was glued with instant adhesive to the sample mount (Ch. 5 gives details of the current experimental procedure). The sample mount is preloaded to the holder by three O-rings.

Two main criteria in designing the sample mount were its stiffness and mass. The sample mount was analyzed for its stiffness using software developed by Slocum[7]. It was determined that with a coupling diameter of 19 mm, using tungsten carbide balls and silicon carbide grooves, the stiffness would be 7.5 MN/m. The mass is important because the natural frequency of the system comprising the piezoelectric tube and sample mount should be greater than the drive frequency. The maximum cutting velocity, 0.3 m/min., corresponds to a (drive) frequency of 500 Hz. Betzig[8] developed a general equation to include the effect of mass loading on the resonant frequency of a piezoelectric tube. The resonant frequency (in the longitudinal direction) of the tube with a mass of 20 grams is 5 kHz. The sample mount system was designed to have a mass less than or equal to 20 grams so that the resonant frequency of the piezoelctric tube would be much greater than the drive frequency. Careful examination of Betzig's development of the determination of the resonant frequency of a piezoelectric tube with a mass on one end show that the equation was derived assuming that the piezoelectric tube was excited in the longitudinal direction with a sinusoidal voltage. This is not the case for cutting; the piezoelectric tube is moved in the transverse direction. It does not seem that the equation Betzig developed is valid for this calculation.

2.3 In-feed Displacement Transducer

An LVDT was first tried as the in-feed displacement transducer but was found to have some problems. The major problem was heat dissipated by the LVDT. This problem made the LVDT unsuitable for this application.

The suitability of a capacitance gage as an in-feed displacement transducer was checked using a modified plane mirror interferometer. The capacitance gage was mounted inside the piezoelectric tube with a lapped aluminum surface on the back of the sample mount holder acting as the target. The capacitance gage used has a resolution of 1 nm. The performance of the capacitance gage inside the tube scanner was evaluated by monitoring the displacement of the PZT tube using the laser and the capacitance gage. A drift test was conducted in a temperature controlled laboratory ($\pm 0.05°C$). The drift of the PZT tube was found to be about 2.5 nm in 86 seconds, as shown in Fig. 2-3. The capacitance gage was also tested by extending the PZT tube by 1 μm and observing the readings of the laser and capacitance gage. Figure 2-4 shows that the laser and capacitance gage agree well. Note the Y axis in Fig. 2-4 is the deviation from 1 μm. Also note that there is a dimensional stabilization that takes place following an initial dimensional change in response to a step input of the applied voltage.

The next criterion for evaluating the capacitance gage was the variation in the capacitance gage voltage output as the PZT tube made the cutting motion. A point along the centerline of the PZT tube will trace out a circular arc during the cutting motion. Using a tube length of 25.4 mm and a cutting length of 10 μm, the maximum depth change during the cutting would be 0.45 nm in the Z direction. Figure 2-5 shows the change in Z displacement during the cutting action, i.e., the PZT tube was moved in the X direction from -5 μm to +5 μm. The change in the Z axis displacement was about 40 nm when the target tilt was removed. This displacement change could have been inherent to the PZT tube or the capacitance gage. Two more experiments were carried out to determine whether the PZT tube or the capacitance gage was causing

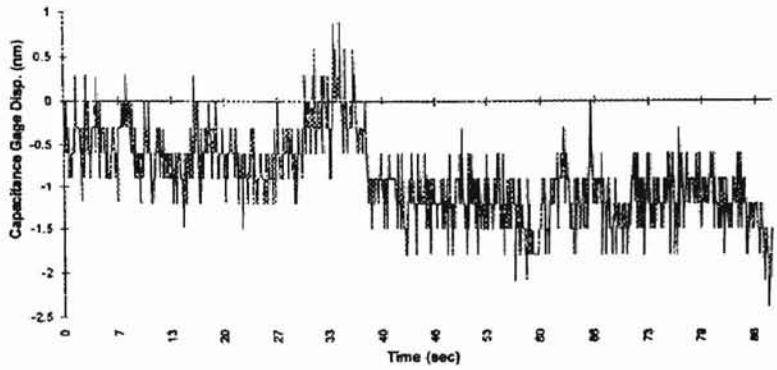

Figure 2-3: Capcitance gage open loop drift test with no voltage applied to the PZT tube (from [1]).

the large change in the Z axis displacement during cutting. Figure 2-6 shows the profile of the capacitance gage face.

Because the profile of the capacitance gage face is a parabolic arc, it might have an effect on the capacitance gage reading when the PZT tube is moved in the X direction. To test this, a gage block set out of square by 0.1° was used as the target for the capacitance gage. Figure 2-7 shows the capacitance gage output as the gage block is moved in the X direction. The slope of the curve corresponds to the slope of the gage block.

To confirm that the parabolic shape traced by the tube scanner was approximately 40 nm in magnitude, the scanning experiment was repeated with the lapped aluminum target mounted on a tilting stage. The tilting stage was adjusted to remove the tilt of the target with respect to the capacitance gage. Figure 2-8 shows that the parabolic shape is about 35 nm which agrees with the previous experiment. This suggests that the circular arc was inherent to the motion of the PZT tube. Thus the capacitance gage was found to be suitable as the in-feed displacement transducer.

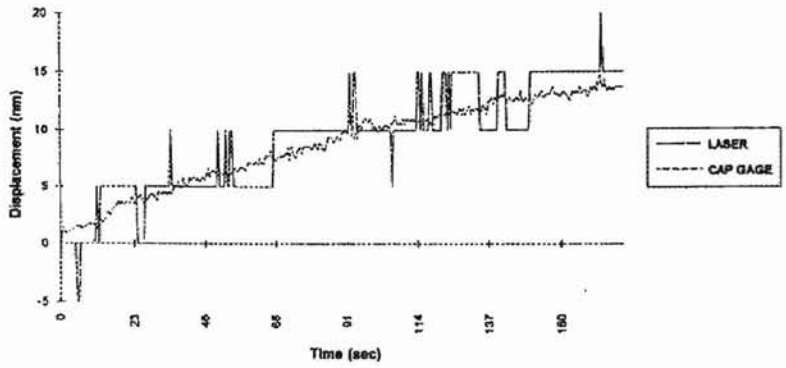

Figure 2-4: PZT tube "creep" with high voltage applied to PZT tube (from [1]).

2.4 Supporting Components of the Instrument

Figure 2-9 shows the electrical components that support the instrument. Originally a 486 personal computer was used to control the motion of the PZT tube, to record the thrust and cutting forces and the position of the PZT tube. In order to perform these functions, the computer has two digital-to-analog, analog-to-digital (D/A) boards in it. An analog signal is needed to control the motion of the PZT tube and the computer requires that the forces and position data to be recorded be a digital signal. The PZT control box contains two high voltage amplifiers that supply the high voltage to the PZT tube X- and Y-quadrants. Recall that motion in the Z direction is obtained by an equal extension of all four quadrants of the PZT tube. The PZT control box also acts as the interface between the computer and the instrument. The output of the capacitance gage goes to the PZT control box then to the computer to record the position of the PZT tube. Originally the cutting and thrust forces were similarly recorded by the computer except that they were first amplified by an amplifier with a gain of about 20. The method of recording the force data has been changed and will be discussed further in Section 3.1.2. The dashed lines in Fig. 2-9 show the setup used for establishing the sample surface. The signal applied to

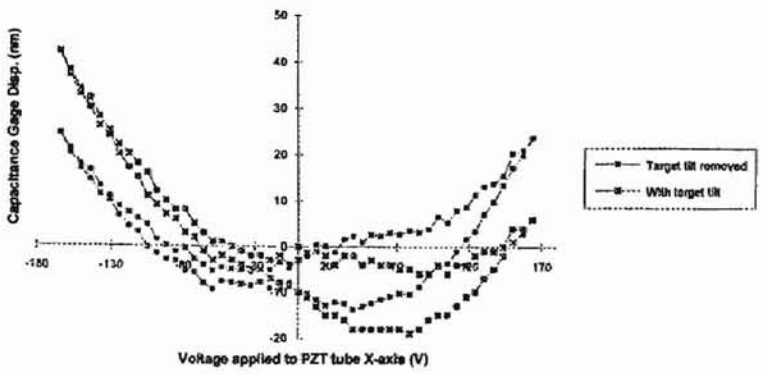

Figure 2-5: Capacitance gage displacement when the PZT tube is moved in the X direction from -5 μm to +5 μm (from [1]).

the PZT tube is a DC signal with a small amplitude sine wave on top of it. The DC component is used to advance the sample towards the tool and the sine wave is used to oscillate the sample. These two signals are summed together in the summing amplifier (gain of 1). A function generator supplies the sine wave to the summing amplifier and it supplies a sine wave to the lockin amplifier to serve as a reference signal.

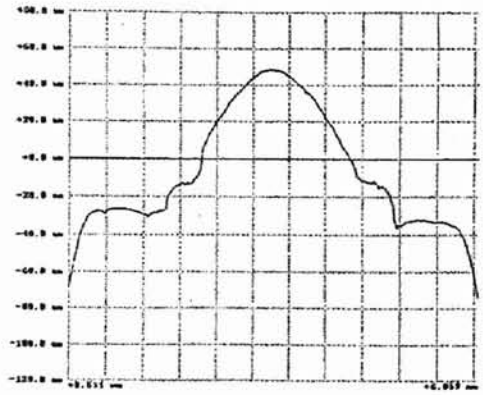

Figure 2-6: Cross-section of the capacitance gage face obtained using a Talystep stylus profilometer (from [1]).

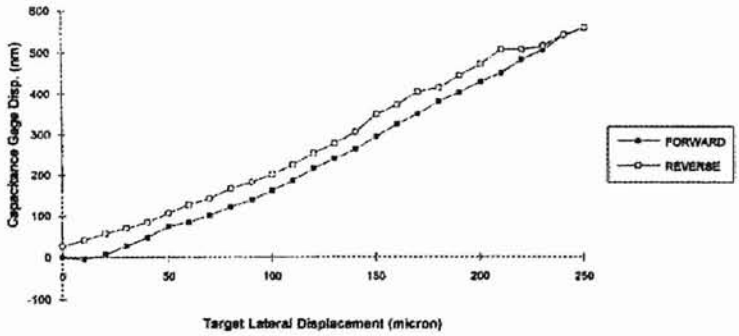

Figure 2-7: Effect of tilted target moved across the capacitance gage (from [1]).

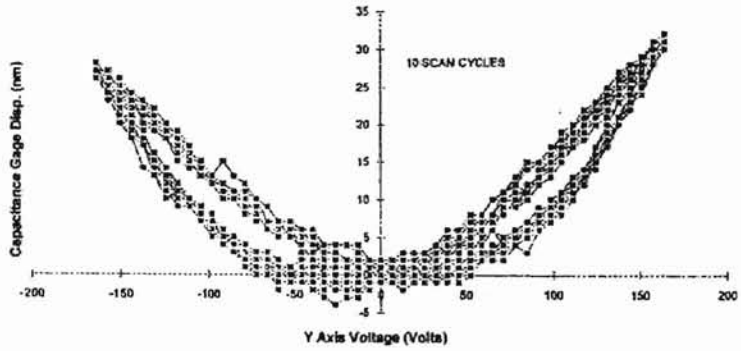

Figure 2-8: Parabolic path traced by PZT tube when scanned over a flat target (from [1]).

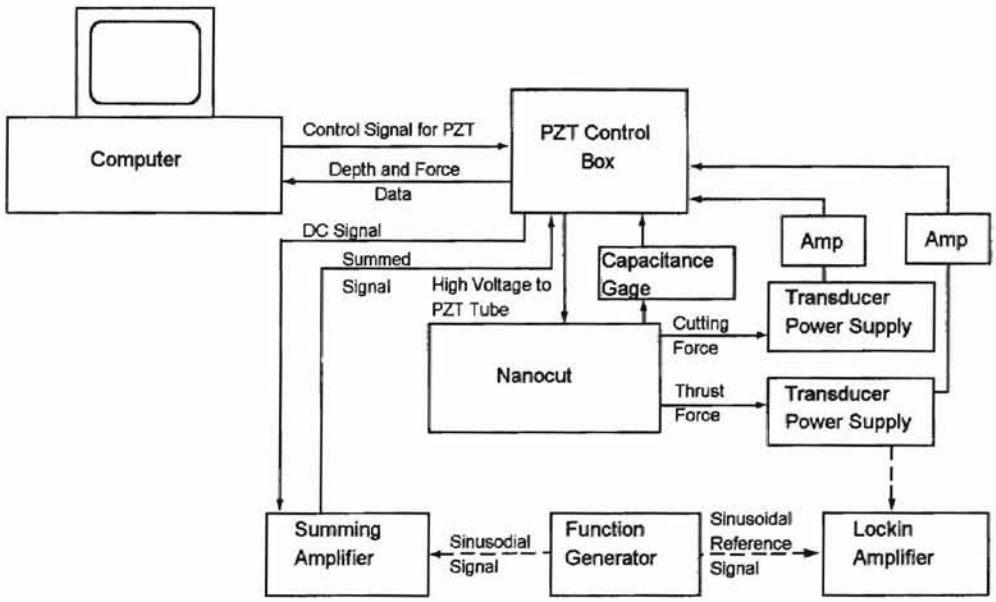

Figure 2-9: Schematic diagram of the original supporting components for the instrument. The dashed lines show the connections that were made for the "Orient" function.

Chapter 3

Modifications and Additions to the Original Design

The instrument, Nanocut, was built at the University of North Carolina at Charlotte where preliminary tests were conducted including indentation tests and scratching tests. The instrument was then delivered to Oklahoma State University where it underwent extensive shakedown testing. As further calibration and testing were performed, several potential modifications and improvements became apparent. They were made either to improve its performance or by necessity and are described below.

3.1 Hardware

3.1.1 D/A Boards

The D/A boards are used to convert the digital signal from the computer to an analog signal to the amplifier that moves the PZT tube. Also, the D/A boards convert the analog signal of the capacitance gage to a digital signal to be recorded by the computer. There are two different D/A boards in the control box, DT 2821 and DT 2823 manufactured by Data Translation, Inc. DT 2823 is a 16 bit board

that was originally used to convert the signal that goes to the Y axis electrodes of the PZT tube. This gave a resolution of 0.15 nm in the Y direction. DT 2821 is a 12 bit board originally used to convert the signal that goes to the X and Z axis electrodes of the PZT. This gave a resolution of 0.77 nm in the Z direction and 2.6 nm in the X direction. The two boards were switched so that DT 2823 (16 bit) is used for the X and Z axis and DT 2821 (12 bit) is used for the Y axis. This enables resolutions of 2.6 nm in the Y direction, 0.15 nm in the X direction and 0.044 nm in the Z direction. This assumes that there is no noise generated by the D/A boards. The DT 2823 board was tested with the differential input shorted and the resulting noise was found to be about 0.15 mV rms [1], which corresponds to about 0.2 nm in either the X or Z direction.

3.1.2 Force Data Collection

The force transducers used in the instrument are piezoelectric force transducers. The response of these transducers to a step input is a rapid rise followed by an exponential decay. The time constant for this decay is about 1 second so the signal decays about 5 % in 50 msec. Figure 3-1 shows the output of a piezoelectric force transducer to a series of step inputs. The force of each step is proportional to the ΔV's. In this figure the force decays to about the same level after each force input but this need not be the case. Originally only one value of force was recorded, the peaks of the curves shown in Fig. 3-1, but it is the change in voltage that is needed to calculate the force not simply the level of the peak voltage. For this reason the force collection was changed to using a digital oscilloscope that can record the data.

Originally, there were two amplifiers used to amplify the voltage of the force transducers before it was sent to the D/A boards. This was to insure that the force signal would exceed the resolution of the D/A boards. The amplifiers are not currently used because of the higher resolution of the oscilloscope and because they add noise to the signal.

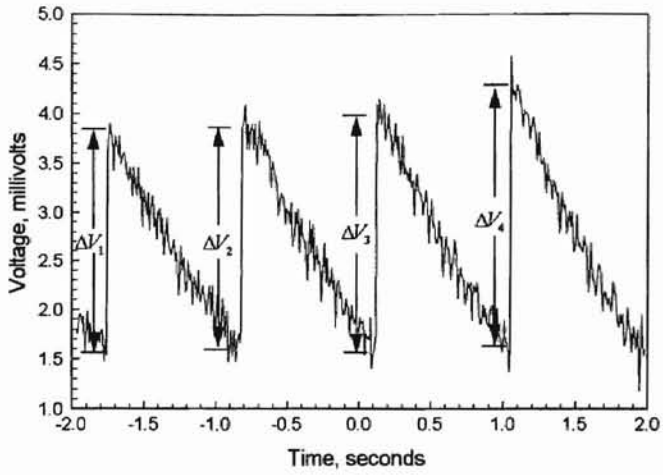

Figure 3-1: Response of transducer to a series of step inputs. The change of the voltage ($\Delta V_1, \Delta V_2$, etc.) is proportional to the force for each input.

3.2 Software

3.2.1 Orient Function

The "Orient" function is used to establish the location of the sample surface. During this procedure, the sample is both oscillated and stepped towards the surface, by a user determined amount. Figure 3-2 shows the programed sample displacement with time. After each step, a pause of 0.5 sec is introduced.

As originally configured, retraction of the sample by 50 nm was performed by manual input to the computer keyboard after the user observed a measured thrust force (voltage) above 0.01 mV. The orient function was automated so that the computer monitors the output of the lockin amplifier, when the signal is above 0.0075 mV the sample is withdrawn 75 nm automatically to eliminate dependence on operator observation. The pullback distance was increased to 75 nm to insure that the sample would not contact the tool because of instrument thermal drift.

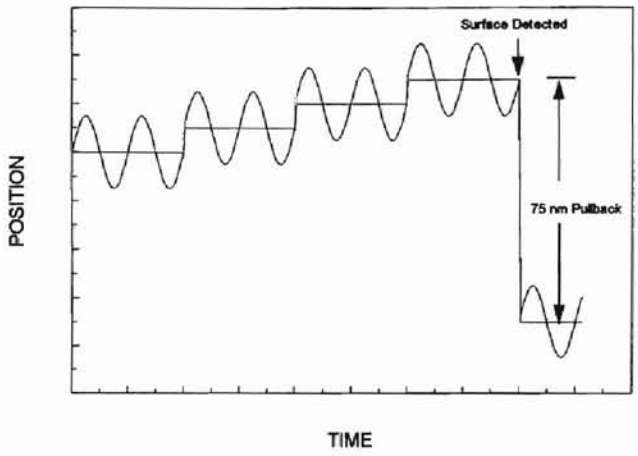

Figure 3-2: Motion of the sample during "Orient" function is a combination of an oscillation and a step input.

3.2.2 Feedback for Position while Indenting

Because of the signal decay of the force transducers, the indentation experiments are performed by making a series of small steps until the desired depth is obtained. During indentation simple feedback is used to hold the PZT tube at the desired position. In the computer program there is a "Hold" function to maintain the position of the PZT tube. As soon as the PZT tube is moved one step the program enters the "Hold" function. When the "Hold" function is started the capacitance gage position is read by the computer. This is the reference position. Then the computer enters a loop in which the capacitance gage position is read, the deviation from the reference position is computed, the PZT tube is moved by the amount of this deviation and then there is a 40 msec pause. This loop is executed forty times. The entire "Hold" function takes about 0.8 sec afterwhich the PZT tube is moved in another step.

Chapter 4

Pre-Experiment Calibrations

4.1 Calibration of Force Transducers

Both the cutting and thrust force transducers were calibrated using deadweights. The force tripod was removed from the instrument and held in a fixture for the calibrations. The preload was adjusted to about 5 N, half the range of the transducer. Both transducers were tested in two modes, "compression increasing" and "compression decreasing". The force tripod showing the location of the deadweight in each mode of loading is shown in Figs. 4-1 and 4-2. In the compression decreasing mode, the deadweight is placed on top of the transducer adding to the compressive load. When the deadweight is removed, the compressive force on the transducer is decreased by the amount of the deadweight. In the compression increasing mode, the deadweight hangs from the transducer decreasing the compressive load on the transducer. When the load is removed, the compressive load on the transducer increases. The deadweights used ranged from 5.2 mN to 490 mN. This is well below the preload of 5 N so the transducer was always in compression.

The deadweights were removed from the transducer ten times with the highest and the lowest values being discarded and the average of the remaining eight taken. Figure 4-3 shows the results of the calibration of the thrust force transducer in the

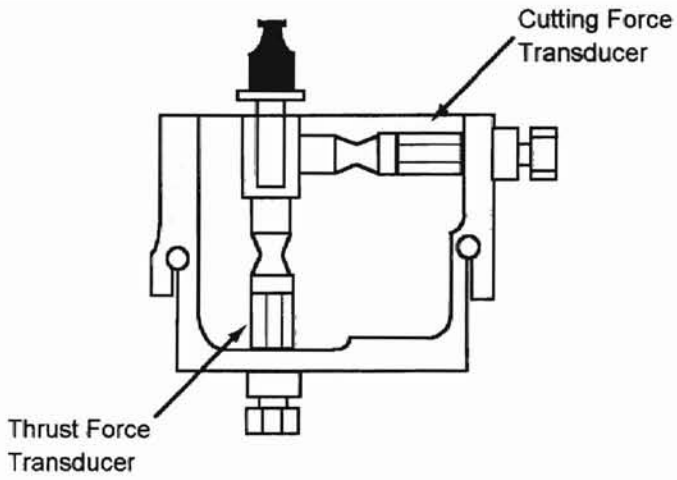

Figure 4-1: Thrust force transducer shown in "compression decreasing" mode of calibration.

compression decreasing mode. The data is very close to linear, especially at lower loads. The calibration constants for the thrust force transducer are 2.09 mN/mV for compression decreasing mode and 2.03 mN/mV for the compression increasing mode. The calibration constants for the cutting force transducer are 2.17 mN/mV for the compression decreasing mode and 2.73 mN/mV for the compression increasing mode.

4.2 Measurement of Indenter Tip Geometry

An atomic force microscope (AFM) was used to measure the tip geometry of the indenter used in these experiments. The AFM uses a probe mounted on a flexible cantilever beam to scan in a raster pattern over the sample surface. The deflection of the cantilever is measured at a fixed number of points along each scan line to reconstruct the sample surface. The image obtained by the AFM is influenced by the size and shape of the cantilever tip as shown in Fig. 4-4. Since this hypothetical surface has infinitely sharp corners, the image obtained at the corners will be an inverted image of the local tip geometry.

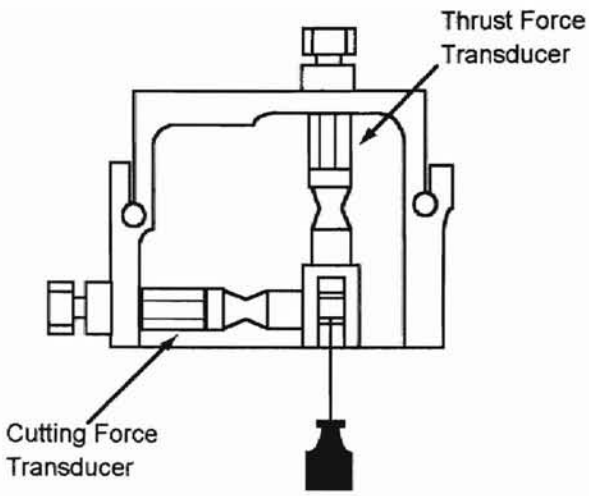

Figure 4-2: Thrust force transducer shown in "compression increasing" mode of calibration.

The cantilever tip is assumed to be part of a sphere. The radius of the sphere is determined by scanning the tip over a surface with a known geometry [9](see App. A). After the indenter is scanned, the size of the cantilever tip may be "subtracted" from the measured geometry to obtain the real surface profile. The computer program used to do this "subtraction" (see App. B) works by moving a point on the image surface by the distance of the radius of the cantilever tip in a direction normal to the image surface[10].

A typical AFM image of the indenter used in the experiments is shown in Fig. 4-5. Note that the scales of the X and Y axes (5 μm) are much larger than the scale of the Z axis (1.3 μm), which makes the indenter look more pointed than it actually is. The geometry of the indenter used (Berkovich indenter) in the experiments is shown in Figure 4-6. The indenter is a three sided pyramid with a 65.3° angle between any face and the vertical axis and a 76.9° between any side and the vertical axis. The cross-sectional area as a function of distance from the tip of the indenter is very close to the area function for a Vickers indenter.

After correcting for the finite size of the cantilever tip, the AFM software is used

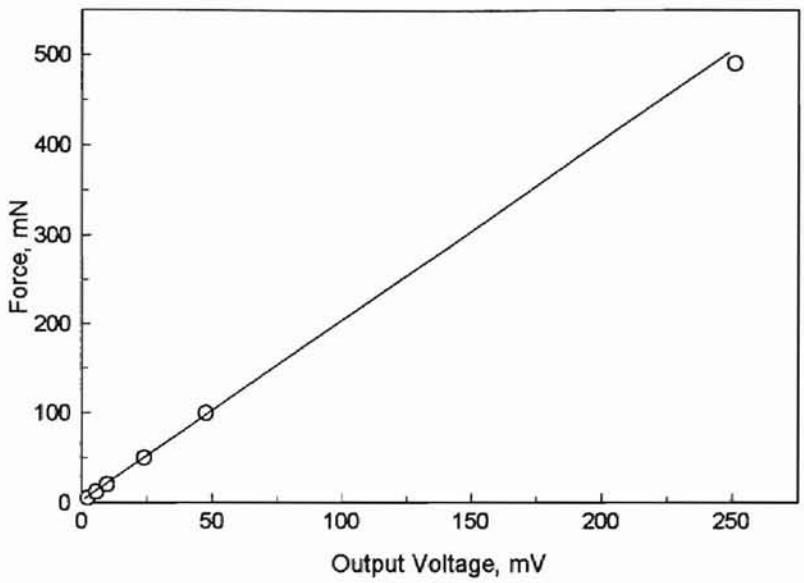

Figure 4-3: Calibration of the thrust force transducer in compression increasing mode. Calibration constant was determined to be 2.09 mN/mV.

to get the bearing ratio for the indenter. The bearing ratio is the percentage of the total surface above a reference plane[11]. The bearing ratio is given as a function of the depth below the highest point of the image. The area as a function of depth is obtained by multiplying the bearing ratio by the total area for each depth. The area function obtained in this manner is a listing of depth and area corresponding to that depth. The distance between depths is about 2.5 nm and linear interpolation was used between the data points.

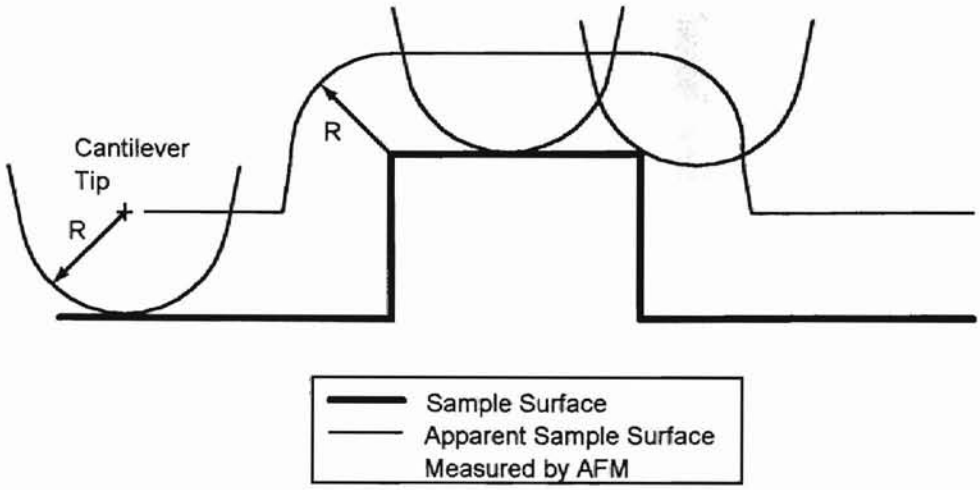

Figure 4-4: Hypothetical sample surface showing the effect of the tip radius on the image obtained by the AFM.

4.3 Measurement of the Usable Frequency Range of the Instrument

It is important that the mechanical resonance of the instrument be much greater than the excitation frequency of the cutting. If this were not the case, the force and depth measurements would be erroneous. The exciting force is caused by either cutting or indenting so this was used as the input force for a frequency response test. The output was the output of the force transducers.

To test the frequency response of the system an indentation experiment was performed. The sample material was fused silica, and a Berkovich indenter was used. The input to the system was the motion of the PZT tube as measured by the capacitance gage and the output was the output of the thrust force transducer. The material sample was first indented to a depth of about 300 nm. Then a pseudo-random signal was applied to the PZT such that the rms amplitude of oscillation of the sample material was about 15 nm peak to valley. This value was chosen to ensure that the loading and unloading would be elastic and the indenter and material

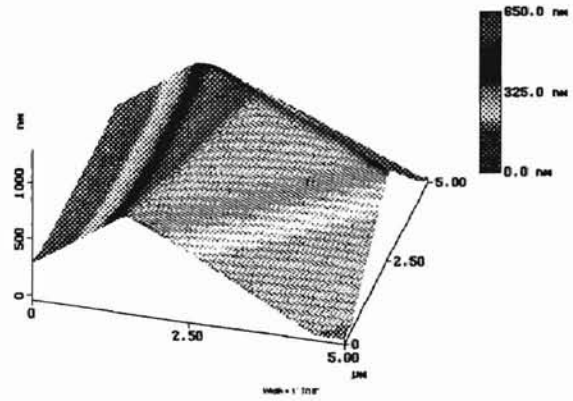

Figure 4-5: AFM image of the indenter used in the experiments.

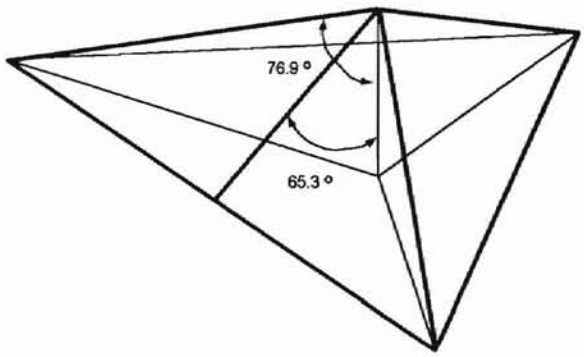

Figure 4-6: Ideal Berkovich indenter.

sample remained in contact. The bandwidth of the pseudo-random signal was 0.03 Hz to about 16 kHz. A spectral analysis of the input and output was performed using *Matlab*. Figures 4-7 and 4-8 show the magnitude and phase of the frequency response of the system. The magnitude is flat up to almost 1000 Hz but above 4000 Hz the magnitude is erratic. The phase diagram is also reasonable up to about 4000 Hz but then the phase becomes erratic. Further testing is needed to confirm these findings but it seems that the instrument can be used up to about 1000 Hz.

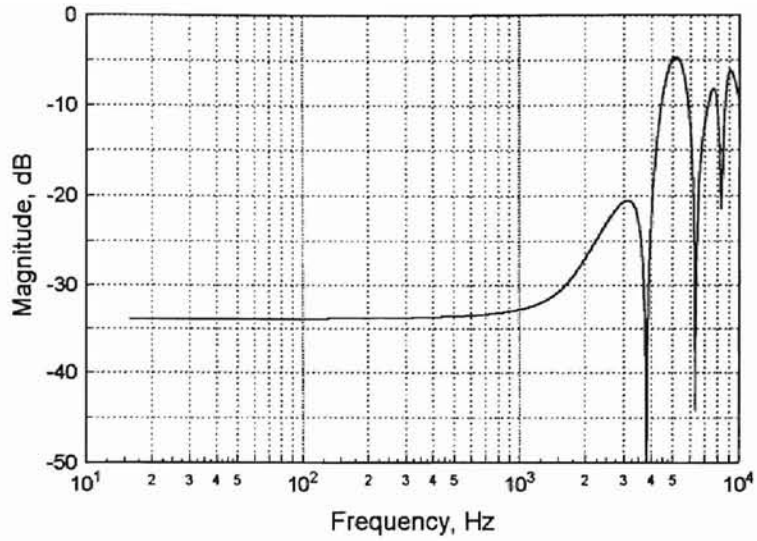

Figure 4-7: Magnitude of the response of thrust force transducer to the motion of the material sample.

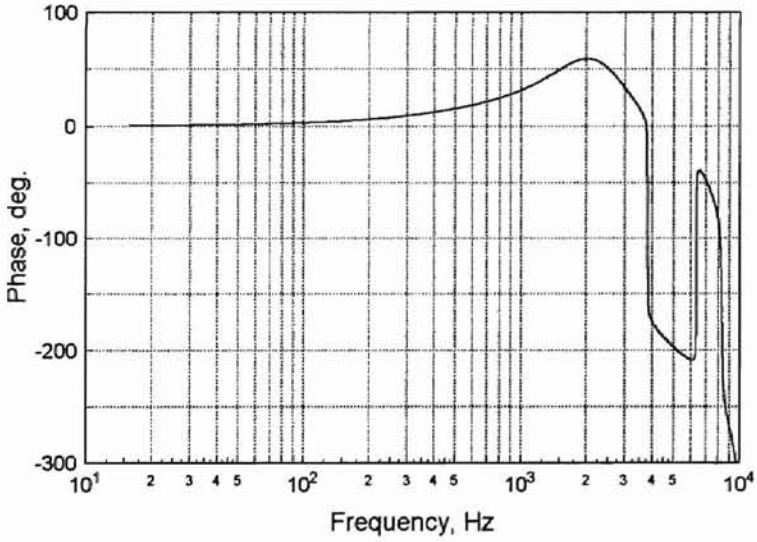

Figure 4-8: Phase of response of thrust force transducer to motion of the material sample.

Chapter 5

Shakedown Experiments

5.1 Procedure

The main purposes of the shakedown experiments were to determine the frame compliance (see Chapter 6) and to measure the elastic modulus of a material and compare it to reported values. To accomplish this nanoindentation experiments were performed. The indenting procedure that was used is outlined in this section.

All of the equipment that supports Nanocut is turned on, including the function generator. This is used for the "Orient" function which locates the surface of the sample. After starting the computer program, the user moves the PZT tube as far away from the indenter as possible to allow for the maximum usable range of the PZT tube.

The sample is mounted to the sample mount using a small amount of glycol thylate. The sample mount is then attached to the sample mount holder with O-rings. The sample is moved by the 80 TPI screw until it is a few millimeters away from the indenter. Looking through an optical microscope, the height of the indenter relative to the top of the sample is estimated. The absolute position of the indenter is not critical, but this check is simply used to ensure that the tip of the indenter is sufficiently far from the edge of the sample. While focused on the indenter, the

sample is moved closer to the indenter by the 80 TPI screw until the mirror image of the indenter can be seen on the sample surface. The lighting of the indenter and sample may have to be adjusted to see the mirror image. The indenter and sample are brought close enough together so that the indenter and the mirror image are nearly touching. Now the "Orient" function of the computer program may be used to establish the sample surface. The "Orient" function requires input from the user for the size of the steps to be taken (usually 5 nm) and the sensitivity of the lock-in amplifier. The output of the capacitance gage is sent to the oscilloscope so that when the sample surface is detected the capacitance gage reading corresponding to the surface can be recorded. If there was not a successful engagement the sample is pulled back as far as possible from the indenter and the sample is moved with the 80 TPI screw closer towards the indenter. Then, the "Orient" function is tried again.

After the location of the sample surface has been determined, indentation can begin. The function generator is turned off and the output of the thrust force transducer is connected to the oscilloscope. The "Indent" function of the computer program is started by the user. The function asks the user for the desired depth of the indentation, the step size going into the sample as well as going out of the sample, and a file name to store the capacitance gage data. The oscilloscope must also be set up to record the force data. The indentation can then be made in the sample.

The loading pattern used in the experiments, as shown in Fig. 5-1, is composed of multiple loadings and unloadings. It is reported that this multiple loading pattern will ensure that the final unloading will be mostly elastic[12]. An experiment was performed to test this and the results will be presented in Chapter 6. The final unloading will be used to calculate both the frame stiffness and the elastic modulus of the material (see Chapter 6).

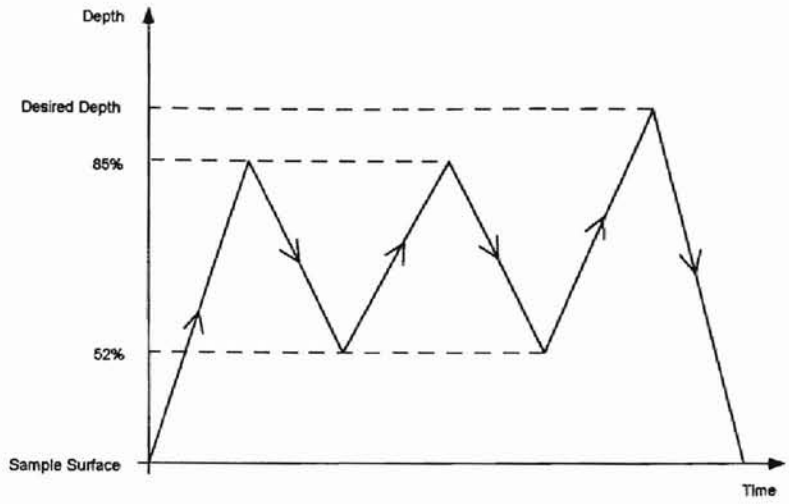

Figure 5-1: Loading pattern used in experiments. The multiple loading is so that the final unloading is mostly elastic.

5.2 Materials and Depths Used in Experiments

Initially test indentations were done on (331) germanium, soda lime glass and fused silica. In the tests used for the calculation of the frame compliance, only fused silica was used. Fused silica is amorphous so there are no orientation effects. The fused silica was chemomechanically polished and cut into 5 mm x 5 mm x 1.8 mm pieces.

The depths used during the indentation experiments were from 400 nm to 1400 nm. The large depths were used because of the procedure used to obtain the stiffness of the frame (see Chapter 6). Currently, for performing indentation the instrument is limited at the lower range (less than 400 nm) because of the noise in the force signal.

5.3 Typical Results

Figure 5-2 shows the load-depth plot for a 1010 nm indentation in fused silica. The multiple loading pattern can be seen. The indentation depth of 1010 nm is the depth under load. When the load is removed the depth of the impression will be about

430 nm, as indicated where the final unloading curve intersects the depth axis. The indentation was done with a step size of 40 nm when going into the indenter and 20 nm when going away from the indenter. Even though one usually thinks of the indenter moving toward the sample, recall that in this instrument it is the sample that moves toward the indenter. These depths were chosen so that when going toward the indenter very few points at small depth would be missed. Recall that the force transducer only measures the change in force from one step so when at small depths if the step size is too small the change in force is also very small and cannot be accurately measured. It was determined that a step size of 40 nm below a depth of 100 nm in fused silica gave an acceptable signal to noise ratio (2 mV/mV). In Fig. 5-2 there is no measured force until about 60 nm. The zero depth position is determined from the procedure to establish the sample surface. The step size moving away from the indenter was chosen so that the number of data points on the final unloading curve would be greater than 20. This is important because the final unloading curve will be curve fit (see Chapter 6.1). The final unloading curve does not precisely intersect the depth axis because there is some error in measurement at each data point. These errors should on average cancel out but might not cancel out each time.

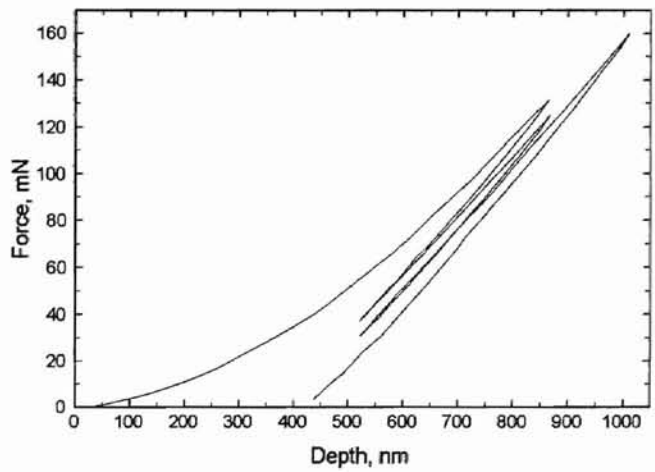

Figure 5-2: Indentation in fused silica with a maximum depth of 1010 nm.

Figure 5-3 shows an AFM image of an indentation in soda lime glass. This is the top view of the indentation looking down into the bottom of the indentation. The maximum depth under load was about 500 nm and the measured depth of the indentation was about 230 nm. The outline of the indentation is not an equilateral triangle which is thought to be because of was some tilt of the sample surface relative to the indenter. The sides of the outline of the indentation are not straight but curved because of the different amount of elastic recovery at the corners and the sides. There is a higher stress at the corners as one would expect so there is less elastic recovery there than elsewhere.

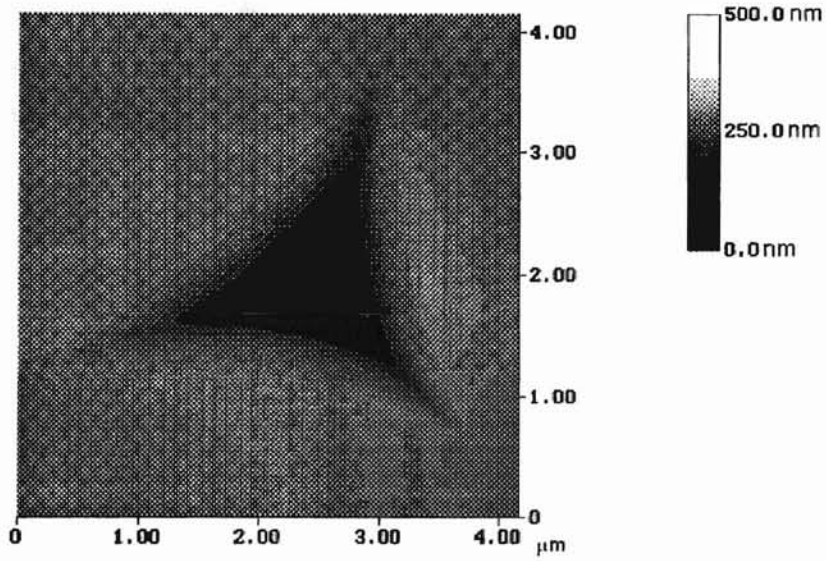

Figure 5-3: Indentation in soda lime glass with maximum depth under load of 500 nm. The measured depth of the impression is 230 nm.

Figure 5-4 shows the top view of an indentation in fused silica. The maximum depth under load was 1000 nm and the measured depth of the impression was about 520 nm. Again the outline of the indentation is not an exact equilateral triangle because of apparent tilting. At the corner towards the bottom of the figure there is a narrowing of the impression that occurs. This may be from a flaw in the surface of

the indenter.

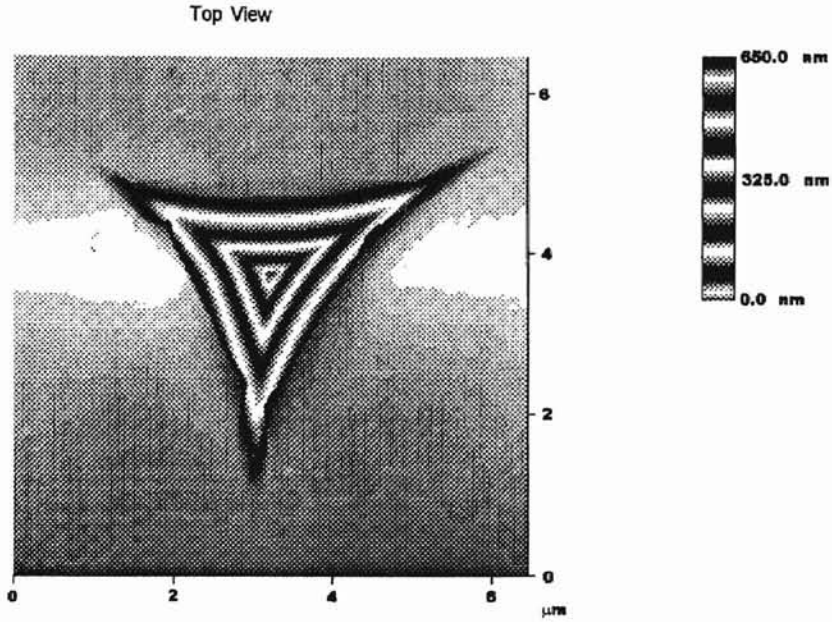

Figure 5-4: Indentation in fused silica with a maximum depth under load of 1000 nm. The depth of the impression made was 520 nm.

An interesting feature of the indentations is shown in Fig. 5-5. The AFM is used in deflection mode, which measures the change in height from one datapoint to the next so that the image shows the surface roughness not the height of surface features. The two extreme peaks in the cross-section are where the indentation begins and ends. The sharp rise in the center of the cross-section is where the two sides of the indentation meet each other. The surface roughness of the indentation is a little bit higher than that of the surface surrounding the indentation. The markers show the maximum peak to valley of the surface roughness of the indentation is 0.862 nm.

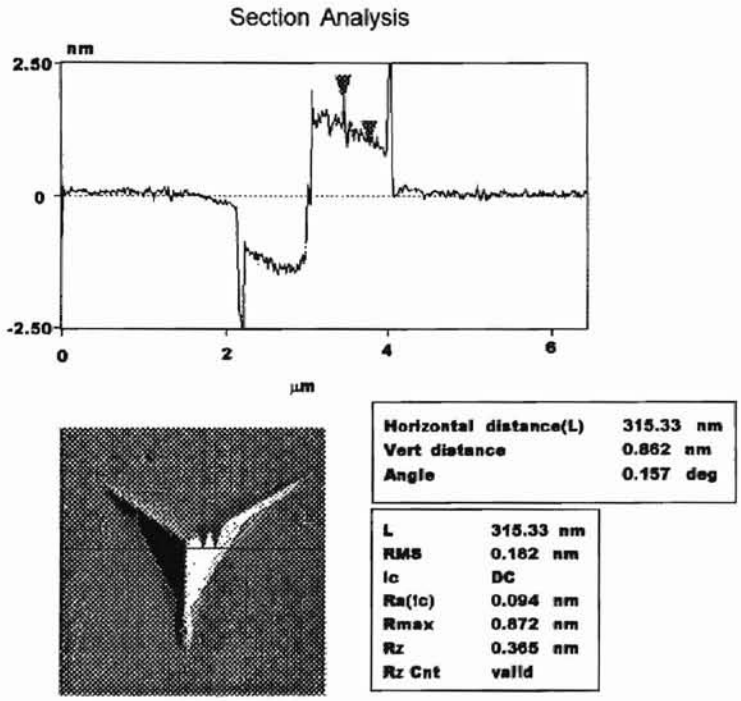

Figure 5-5: Cross-section of same indentation as in Fig. 5-4. The AFM is used in deflection mode so the image shows the surface roughness not the height of the sample.

Chapter 6

Analysis of Data and Discussion of Results

6.1 Analysis of Data

The analysis of the data obtained by nanoindentation using the instrument consists of two parts: determination of the stiffness of the instrument (or the frame compliance) and the determination of the elastic modulus of the material on which indentation was performed. The method of Oliver and Pharr [12] was used extensively with only slight modifications. The basic equations for the determination of the elastic modulus of the material are based on a mathematical model of a rigid punch indenting an elastic half-space. Most all instruments used for indentation measure the force on the indenter, P, and the depth relative to a reference plane, h. Figure 6-1 is a schematic diagram of a typical load versus depth graph showing both loading and unloading. The material stiffness is obtained from:

$$S = \frac{dP}{dh} = \frac{2}{\sqrt{\pi}} E_r \sqrt{A} \tag{6.1}$$

where S = slope of unloading curve at maximum depth

E_r = reduced elastic modulus of the sample

A = area of contact

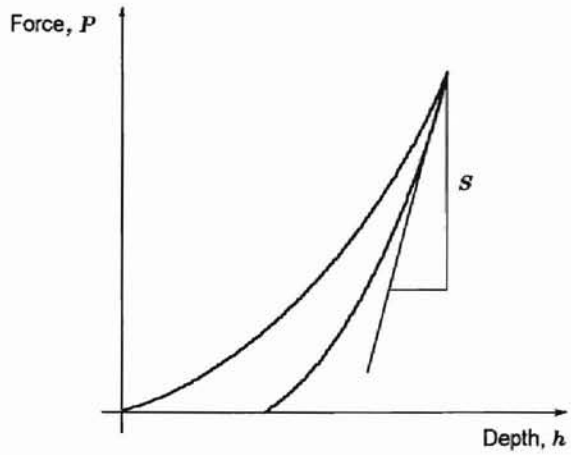

Figure 6-1: Schematic diagram of the unloading curve showing the slope, S, at the maximum depth.

The area of contact is the projected area of sample-indenter contact. Figure 6-2 shows the contact depth h_c at which the area of contact is calculated. In part (a) of the figure, the indenter is loaded onto the material sample, and (b) shows the material sample after the indenter has been removed. The contact depth is the depth measured from the tip of the indenter to the highest point where the indenter and material sample are in contact. The figure also shows the final depth, h_f and the displacement of the surface at the perimeter, h_s.

The quantity E_r, in Eq. 6.1, appears because the indenter is not perfectly rigid so the elastic modulus measured is a combination of the elastic modulus of the material sample and the indenter. The elastic modulus of the material can be obtained from[12]:

$$\frac{1}{E_r} = \frac{(1-\nu^2)}{E} + \frac{(1-\nu_i^2)}{E_i} \tag{6.2}$$

where E and E_i are the elastic moduli for the sample and the indenter respectively

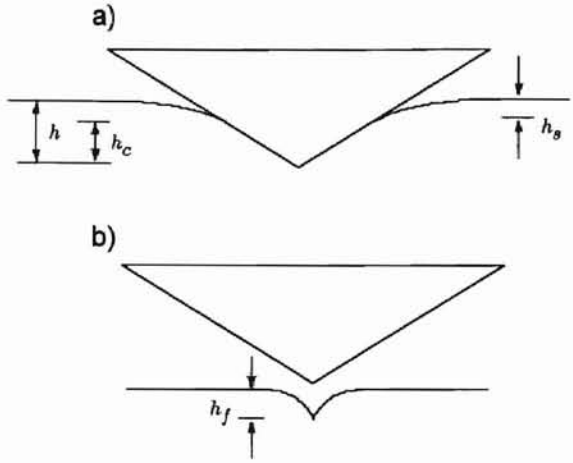

Figure 6-2: Definition of depths used in the text. a) shows the indentation under load, b) shows the indentation after the load has been removed.

and ν and ν_i are Poisson's ratios for the sample and indenter. For the case of indenting fused silica with a diamond indenter the term corresponding to the indenter accounts for 6% of the total. Also, Eq. 6.1 does not take into consideration the frame compliance of the instrument.

One technique of determining the slope of the unloading curve is to draw the straight line asymptote to the upper one third of the unloading curve[13]. This assumes that the contact area does not change during the upper one third of the unloading. Oliver and Pharr[12] suggest that a better technique is to curve fit the unloading curve with the following equation:

$$P = \alpha(h - h_f)^m \tag{6.3}$$

where P = measured force

h = depth

α, m, h_f = constants to be determined by curve fit

Physically h_f is the depth of the impression left in the sample after the load has been

removed, as shown in Fig. 6-2. The depth of the impression could also be measured from the AFM image of the indentation but it is sometimes difficult to measure this value. The image of the sample surface may be tilted or depending on the cross section taken the value of h_f may vary by up to 40 nm. The values obtained by the curve fit are also within 40 nm of the value obtained by measuring the AFM image, so the values obtained from the curve fit are used. The slope at the maximum load is obtained by analytically differentiating Eq. 6.3 and using all the known values, which include the peak load and depth, the final depth (h_f), α and m.

Recall that in the actual experiments a multiple loading-unloading procedure is used. A comparison of the slope of the first and third unloading curves was done for fused silica. Table 6.1 shows that the slope of the first unloading curve is always less steep than that of the final unloading curve. From Eq. 6.1, a higher slope means a higher elastic modulus. Because the final unloading curve is mostly elastic, it gives a higher value of the unloading slope.

The total measured compliance is the inverse of the total measured stiffness. The total measured compliance contains both a contribution from the sample material and the indenting instrument. When indenting the measured depth is not the actual depth because some of this displacement is a result of the compression of the instrument. The compression of the instrument can be given by either the instrument compliance (frame compliance) or its stiffness (frame stiffness). Since it influences the determination of the elastic modulus, accurate determination of the frame compliance is very important. If one assumes a frame compliance of 1.13 nm/mN [12] then this represents about 34%-40% of the total measured compliance for indentations in fused silica over the range of depths of 1000 nm to 1400 nm under load. The method used to obtain the frame compliance is given below.

The instrument and the specimen are modelled as two springs in series, so the compliance of each element is summed to get the total compliance.

Max. Depth, nm	Slope of First Unloading	Slope of Final Unloading
501	0.174	0.193
507	0.186	0.196
621	0.193	0.199
615	0.212	0.233
640	0.193	0.198
717	0.204	0.205
727	0.206	0.230
710	0.187	0.209
814	0.231	0.247
839	0.238	0.261
831	0.213	0.233
932	0.235	0.260
926	0.250	0.272
937	0.240	0.257
1019	0.255	0.280
1017	0.272	0.285
1021	0.236	0.268

Table 6.1: Comparison of the slope of the unloading curve on the first and the final unloading

$$C = C_f + C_s \tag{6.4}$$

where C = total measured compliance

C_f = frame compliance

C_s = compliance of the specimen

The compliance of the specimen, C_s, is the inverse of Eq. 6.1. Substituting into Eq. 6.4 results in:

$$C = C_f + \frac{\sqrt{\pi}}{2E_r}\frac{1}{\sqrt{A}} \tag{6.5}$$

The total measured compliance C is a linear function of $A^{-1/2}$; the Y intercept is the frame compliance, C_f. Better estimates of the frame compliance will be obtained with larger A values so that the second term in Eq. 6.5 is small. The area, A, is obtained

from the area function of the indenter and the contact depth. Figure 6-2 shows the contact depth, h_c, the total indentation depth under load, h, the final depth of the impression in the sample, h_f, and the displacement of the surface at the perimeter, h_s. It is the contact depth that is used in the area function to determine the area used in Eq. 6.5 since this is the area that is actually supporting the load.

The contact depth is determined from the unloading curve as follows. The contact depth is related to the maximum depth of the indentation, h_{max}, by:

$$h_c = h_{max} - h_s \tag{6.6}$$

The maximum depth is measured during indentation and h_s can be estimated from Sneddon's expression for the shape of the surface outside the perimeter of contact[14].

$$h_s = \frac{(\pi - 2)}{\pi}(h - h_f) \tag{6.7}$$

Sneddon analyzed an elastic sample so instead of $(h - h_f)$, the elastic depth[12] in Eq. 6.7, he had just h. Also from Sneddon,

$$(h - h_f) = 2\frac{P_{max}}{S} \tag{6.8}$$

where P_{max} = the maximum load

Equation 6.8 is substituted into Eq. 6.7 to obtain an expression for h_s.

$$h_s = \frac{2(\pi - 2)}{\pi}\frac{P_{max}}{S} \tag{6.9}$$

The right hand side of Eq. 6.9 is determined completely by the unloading curve. Using Eqs. 6.9 and 6.6 the contact depth can be obtained, viz.

$$h_c = h_{max} - \frac{2(\pi - 2)}{\pi}\frac{P_{max}}{S} \tag{6.10}$$

Using the contact depth and the area function obtained from the AFM image of the

indenter, the contact area can be obtained.

Rewriting Eq. 6.4 in terms of the specimen stiffness, S_s, the frame compliance, C_f, and the total measured stiffness, S_t:

$$S_s = \frac{S_t}{1 - S_t C_f} \tag{6.11}$$

This is the stiffness that is used in Eq. 6.1 along with the contact area to determine the reduced elastic modulus. After the frame compliance is determined, the elastic modulus of the specimen can be determined.

6.2 Results

Before the elastic modulus of the material may be estimated the frame compliance of the instrument must be determined. The frame compliance is determined from a graph of the total measured compliance versus contact area$^{-1/2}$ (see Sec. 6.1). The contact area is obtained from the area function of the indenter (from the AFM image) and the calculation of the contact depth h_c. The contact depth is the depth that is used in the area function to determine the contact area. Figure 6-3 shows the total measured compliance vs. the contact area$^{-1/2}$ for indentations in fused silica for a series of experiments performed on three diferent days. The depths of the indentations are 1000 nm, 1200 nm and 1400 nm under load. Four indentations were made at each depth and then this was repeated twice. The maximum depth was chosen to avoid fracture of the fused silica. Other investigators have reported the onset of fracture in fused silica to be at about 2.5 μm[15]. Smaller depths were not used because small scatter in the data at small depths (to the right of the graph) can have a large effect when extrapolated to the compliance axis. The intercept of the compliance axis is the frame compliance, about 0.32 nm/mN. This frame compliance is then used in the determination of the elastic modulus of the material to account for the displacement of the frame while indenting. The measured frame compliance is better than the

reported value for a commercial nanoindenter of 1.13 nm/mN[12] and close to the value of a new commercial nanoindenter of 0.5 nm/mN[16].

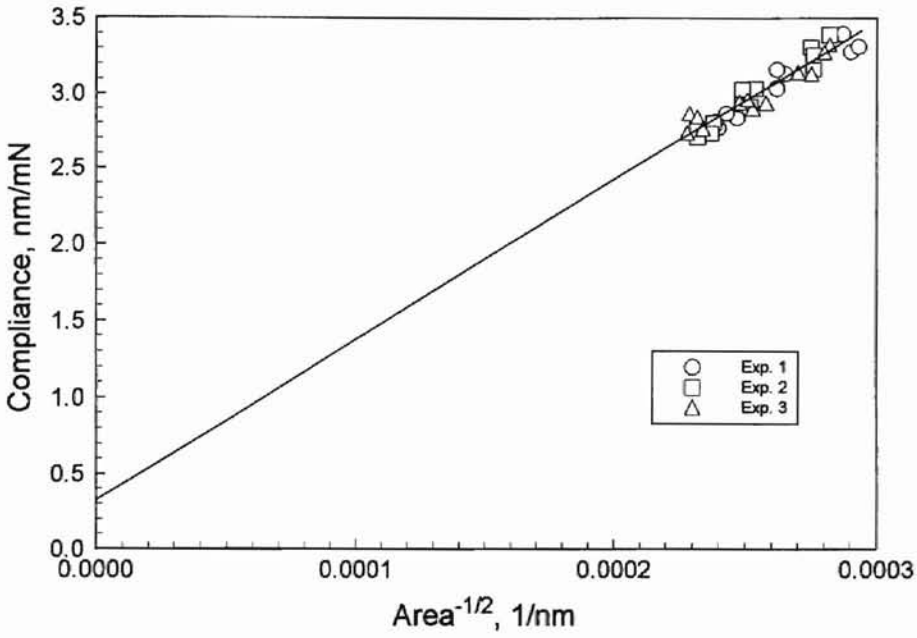

Figure 6-3: Total measured compliance versus contact area$^{-1/2}$. The frame compliance is the intercept of the compliance axis, about 0.3 nm/mN.

Using the value of 0.32 nm/mN for the frame compliance, the elastic modulus and the hardness of the sample material can be determined. Figure 6-4 shows the hardness as a funcition of the contact depth. The depth under load was 800 nm, 1000 nm, 1200 nm, 1400 nm. The average value of hardness is 12.7 GPa which is close to the 9 GPa value reported by Oliver and Pharr [12]. There appears to be a slight decrease in the hardness at smaller depths.

Figure 6-5 shows the elastic modulus as a function of the contact depth for indentations made in fused silica. The depths under load of the indentations are 800 nm, 1000 nm, 1200 nm, and 1400 nm. There are twelve indentations at each depth. The average value of the elastic modulus is 85.3 GPa. The reported value for the elastic modulus of fused silica is 72-74 GPa[17]. One possible cause of the non-repeatability

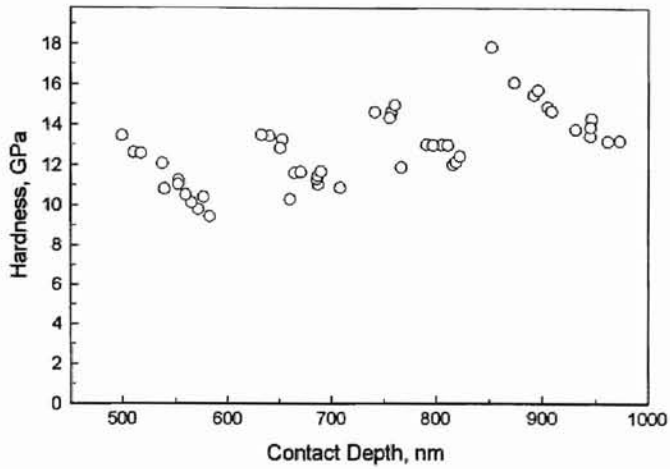

Figure 6-4: Hardness vs. contact depth for fused silica assuming the frame compliance is 0.32 nm/mN.

is the sample mounting. The amount and distribution of the glycol phthalate between the material sample and the sample mount will change for each sample. Also there may be slight tilting between the indenter and the material sample which is not repeatable. The average value of the data is about 15% greater than the reported values. Possible causes of this error are the errors in the measurement of either the force or the depth or both. The next section details an analysis of the errors.

6.3 Error Analysis

There are two main sources of measurement error in this experiment, the force transducer and the capacitance gage. Even though the errors in these measurements are small, they can be magnified because of the mathematical manipulation that is done. Consider a value Q computed from measured values $x_1, x_2, ..., x_i$, that is:

$$Q = f(x_1, x_2, ..., x_i) \tag{6.12}$$

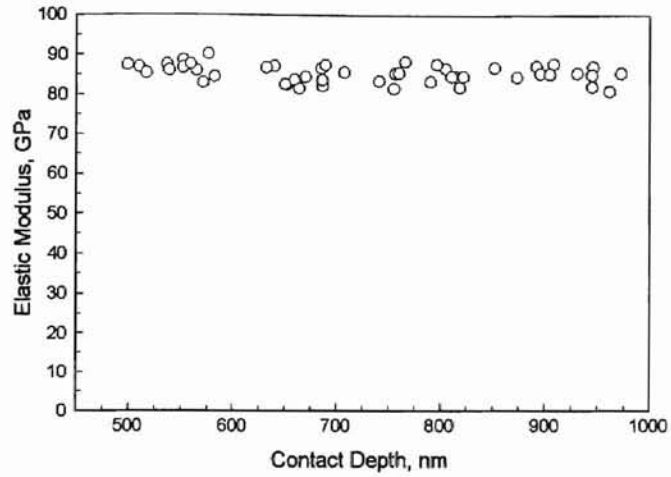

Figure 6-5: Elastic modulus vs. contact depth for fused silica assuming the frame compliance is 0.32 nm/mN. The reported value of the elastic modulus of fused silica is 72-74 GPa [17].

The error in Q can then be calculated from[18]:

$$\Delta Q = \sqrt{\left(\frac{\partial Q}{\partial x_1}\right)^2 (\Delta x_1)^2 + \left(\frac{\partial Q}{\partial x_2}\right)^2 (\Delta x_2)^2 + ... + \left(\frac{\partial Q}{\partial x_i}\right)^2 (\Delta x_i)^2} \tag{6.13}$$

where Δx_i = error in measurement of x_i

ΔQ = error in calculated value Q

The measurement of the slope of the unloading curve is affected by both the error in the force measurement and the error in the depth measurement, Eq. 6.14.

$$\frac{dP}{dh} = \alpha m(h - h_f)^{m-1} = Pm(h - h_f)^{-1} \tag{6.14}$$

Applying Eq. 6.13,

$$\Delta S = \sqrt{\left(\left|\frac{\partial S}{\partial h}\right| \Delta h\right)^2 + \left(\left|\frac{\partial S}{\partial P}\right| \Delta P\right)^2} \tag{6.15}$$

where $S = \frac{dP}{dh}$

Similarly the error in h_c and E_r are calculated as follows. The equation for the contact depth, h_c, as a function of the maximum depth under load, the slope, and the maximum load is (Eq. 6.9):

$$h_c = h_{max} - 0.72\frac{P_{max}}{S} \tag{6.16}$$

So the error in the contact depth is:

$$\Delta h_c = \sqrt{\left(\left|\frac{\partial h_c}{\partial h_{max}}\right|\Delta h_{max}\right)^2 + \left(\left|\frac{\partial h_c}{\partial P_{max}}\right|\Delta P_{max}\right)^2 + \left(\left|\frac{\partial h_c}{\partial Y}\right|\Delta S\right)^2} \tag{6.17}$$

The error in the contact depth can then be used to determine the error in the contact area. It is assumed that the error in the measurement of the area function is much less than the error in the measurement of the force or the depth because the error in the AFM measurement is less than about 3%. The reduced elastic modulus, E_r, is given by the following:

$$E_r = \frac{\sqrt{\pi}}{2}\frac{S}{\sqrt{A}} \tag{6.18}$$

This equation can be used to obtain the error in the reduced elastic modulus.

$$\Delta E_r = \sqrt{\left(\left|\frac{\partial E_r}{\partial S}\right|\Delta S\right)^2 + \left(\left|\frac{\partial E_r}{\partial A}\right|\Delta A\right)^2} \tag{6.19}$$

The elastic modulus is related to the reduced elastic modulus by the following (Eq. 6.2):

$$\frac{1}{E_r} = \frac{1-\nu^2}{E} + \frac{1-\nu_i^2}{E_i} \tag{6.20}$$

The i subscripts refer to the indenter material properties and the ν and E are for the

% Error in Force	% Error in Depth	Error in Elastic Modulus, GPa
3	3	6.75
5	3	8.2
6	3	9.0
5	5	11.5

Table 6.2: Error in elastic modulus because of errors in the force and depth measurements

material itself. The error in the elastic modulus is:

$$\Delta E = \sqrt{\left(\left|\frac{\partial E}{\partial E_r}\right| \Delta E_r\right)^2 + \left(\left|\frac{\partial E}{\partial \nu}\right| \Delta \nu\right)^2} \tag{6.21}$$

The variations in the indenter material properties are small compared to the errors in the reduced modulus so they are assumed to be zero. Also the second term under the radical in Eq. 6.21 is found to be very small and is neglected when the error in the elastic modulus is calculated. Table 6.2 shows the error in the elastic modulus for various combinations of error in the force measurement and the depth measurement. Based on the repeatability of the force transducers and the calibration of the capacitance gage a reasonable assumption for the error in both measurements is 5%. Using this assumption the error in the elastic modulus is 11.5 GPa. Recall that the average measured modulus of elasticity was 85.3 GPa and the value of the modulus reported in the literature is 72-74 GPa[17].

Chapter 7

Conclusion

7.1 Summary

Shakedown experiments of an instrument for nanocutting and nanoindenting were presented. The instrument was designed at the University of North Carolina at Charlotte under a collaborative study on the mechanics of material removal. The sample material can be moved in three orthogonal direction by a PZT tube which enables a cutting depth from a few nanometers to two microns. The motion of the sample material is measured by a capacitance gage which has a resolution of 1 nm. The force on the tool or indenter is measured by two piezoelectric transducers, one in the thrust direction and one in the cutting direction. Forces from 0.4 mN to 5 N can be measured in either the cutting or thrust direction.

Some modifications to the instrument were made. There are two D/A boards that are used in the control box, one for the X and Z axes the other for the Y axis. Originally the board controlling the Y axis was a 16 bit board and the board controlling the X and Z axes was a 12 bit board. This configuration was changed so that the 16 bit board controls the X and Z axes and the 12 bit board controls the Y axis. The force data is collected by a digital oscilloscope. This is so that the voltage change of each step in the indentation process can be recorded. The software

that controls the instrument was changed also. An "Orient" function was added so that the process of establishing the sample surface would not depend on the user. A simple feedback system was used for indentation to hold the position of the material sample in between steps.

Pre-experiment calibrations including the calibration of the piezoelectric force transducers were performed. Both transducers were tested in compression increasing mode and compression decreasing mode. The indenter was also carefully measured taking into consideration the finite size of the cantilever tip.

Preliminary indentations were made in (331) germanium, soda lime glass and fused silica. Fused silica was used as the material for the determination of the frame compliance and to check the validity of its elastic modulus. The depth of the indentations under load was from 800 nm to 1400 nm for the fused silica and down to 400 nm for the soda lime glass and germanium. A multiple loading-unloading pattern was used to ensure that the final unloading curve was mostly elastic. The analysis of the data mainly followed the method of Oliver and Pharr[12]. The frame compliance was calculated to be 0.32 nm/mN which is similar to the value (0.5 nm/mN) for a commercially available nanoindenter[16]. The average value of the elastic modulus for fused silica was calculated to be 85.3 GPa which is about 15% higher than the values reported elsewhere[17]. One possible explanation for the difference could be the errors in the force and depth measurements. A reasonable assumption for the error of both the force and depth measurement is 5%. This error could account for an 11.5 GPa difference in elastic modulus.

7.2 Future Work

Better methods for performing the calibrations for both the force transducers and the capacitance gage are needed. Currently the force tripod is removed from the instrument to calibrate the force transducers. An improvement would be to calibrate

the force transducers with the force tripod in the instrument. Because the slides of the force tripod are filled with a replicating agent the force tripod fits snugly on the precision shafts. The force required to remove and install the force tripod may change the preload on the transducers and thus affect the calibration constant. Also when removing the deadweights, there may be an impulse from uneven removal of the deadweights. The capacitance gage should also undergo recalibration. The capacitance gage was calibrated at UNCC with a laser interferometer. The capacitance gage should again be calibrated with a laser interferometer or similar instrument.

Bibliography

[1] S. Balasubramaniam. Design of a nanometric cutting instrument. Master's thesis, University of North Carolina at Charlotte, 1995.

[2] B. Boudreau. *Near-Field Thermal Imaging of Surfaces Below the Diffraction Limit.* PhD thesis, Michigan Technological University, Houghton, MI.

[3] D. A. Lucca and Y. W. Seo. Effect of tool geometry on energy dissipation in ultraprecision machining. *Annals of the CIRP*, 42:83–86, 1993.

[4] *PCB Piezotronics Force Transducer Catalog.*

[5] L. J. Bredell. Design, construction snd calibration of an impulse dynamometer. *Measurement Science and Technology*, 1:977–979, 1990.

[6] J. M. Paros and L. Weisbord. How to design flexure hinges. *Machine Design*, pages 151–156, Nov. 1965.

[7] A. H. Slocum. *Precision Machine Design.* Prentice Hall: Englewood Cliffs, NJ, 1992.

[8] E. Betzig. *Non-Destructive Optical Imaging of Surfaces with 500 Angstrom Resolution.* PhD thesis, Cornell University, 1988.

[9] D. A. Lucca, Y.W. Seo, and R.L. Rhorer. Aspects of surface generation in orthogonal ultraprecision machining. *Annals of the CIRP*, 43(1):43–46, 1994.

[10] R. Chicon, M. Ortuno, and J. Abellan. An algorithm for surface reconstruction in scanning tunneling microscopy. *Surface Science*, 181:107–111, 1987.

[11] Digital Instruments, Inc. Santa Barbara, CA.

[12] W. C. Oliver and G. M. Pharr. An improved technique for determining hardness and elastic modulus using load and displacement sensing indentation experiments. *Journal of Materials Research*, 7(6):1564–1583, 1992.

[13] M. F. Doerner and W. D. Nix. A method for interpreting the data from depth-sensing indentation instruments. *Journal of Materials Research*, 1(4):601–609, 1986.

[14] I. N. Sneddon. The relation between load and penetration in the axisymmetric Boussinesq problem for a punch of arbitrary profile. *International Journal of Engineering Science*, 3:47–57, 1965.

[15] R. F. Cook and G. M. Pharr. Direct observation and analysis of indentation cracking in glasses and ceramics. *Journal of the American Ceramic Society*, 73:787–817, 1990.

[16] Nano Instruments, Inc. Oak Ridge, TN.

[17] J. F. Shackelford, W. Alexander, and J. S. Park, editors. *CRC Materials Science and Engineering Handbook*. 2nd edition, 1994.

[18] J. B. Kennedy and A. M. Neville. *Basic Statistical Methods for Engineers and Scientists*. IEP, 2nd edition, 1976.

Appendix A

Characterization of Cantilever Tip Geometry

Characterization of the cantilever tip used in the AFM imaging of the diamond indenter was performed according to the procedure described more fully elsewhere[9]. A brief outline of this procedure is presented here. The cantilever tip is a pyramid with a square base having a rounded portion at the apex of the pyramid. This rounded portion is assumed to be spherical.

Commercially available carboxylate microspheres with a diameter of 519 nm are used as the sample. The carboxylate microspheres originally are suspended in water. A small amount of the solution containing the microspheres are put on a freshly cleaved mica surface where the water is allowed to evaporate. Some of the microspheres will assume a close packed arrangement. An area where the microspheres are close packed is then scanned by the AFM. A representative microsphere is selected and its cross section is measured in each of the three close pack directions. This distance is the diameter of the microsphere independent of the size of the cantilever tip. This is because the minimum points will be where any two microspheres touch. An average of the three diameters is taken and this is taken as the diameter of the microsphere.

A cross section of the selected sphere is then curve fit with a simple computer program. The program computes the sum of the absolute value of the errors for a given center and radius. The user gives an initial guess for the center and radius of the arc and then the computer executes nested loops where the center is moved ± 50 nm in the X and Y directions and the radius is varied from the initial guess to the initial guess plus 110 nm. The combination of X center location, Y center location and radius that gives the smallest absolute value of errors is taken to be the best fit of the data. To obtain the radius of the cantilever tip, the radius of the microsphere is subtracted from the radius of the curve fit by the computer.

Appendix B

Computer Program for the Deconvolution of AFM Images

The following computer program is used to deconvolve an image obtained from the AFM. This program is based on geometric relationships presented elsewhere [10]. Every point in the AFM image is composed of an x, y, and z coordinate where z is the height. At every point the computer program calculates the slope of the tangent line to the surface in both the X and Y directions using a five point central difference formula. These slopes are used to calculate the normal to the surface and the original datapoint is moved along this normal a distance equal to the cantilever tip radius. The method assumes that the cantilever tip is spherical, and that the radius of the tip is known.

The computer program has two parts, the main program and a file for the calculations. The main program reads the data, then prompts the user for input of variables used in the caluculation of the height of the data. Then the program goes through all of the x, y combinations so that every point in the original image is operated on. Finally in the main program the data is written to a file. The other file contains the functions that perform all of the calculations on the data such as the slope.

```
#include <stdio.h>
```

```
#include <math.h>
#include "nrutil.h"
#include "convolution_calc.h"
/* THIS PROGRAM IS BASED ON THE PAPER "AN ALGORITHM FOR SURFACE
RECONSTRUCTION IN SCANNING TUNNELING MICROSCOPY" BY R. CHICON,
M. ORTUNO, AND J. ABELLAN IN SURFACE SCIENCE v. 181 (1987) pgs. 107-111 */
main()
{
 int i,j,k;
 float **z,**znew,zsens,zatten,scan_size,zmax,zheight;
 float slope_x,slope_y,radius,delta_z,*zorder;
 float area_per_point, depth, area;
 int delta_x,delta_y;
 FILE *fp,*ofp,*ofp2;
/* DATA FROM NANOSCOPE IS STORED IN MATRIX CALLED z, DECON-
VOLVED DATA WILL BE STORED IN MATRIX CALLED znew */
 zorder = vector(0,57600);
 z = matrix(0,255,0,255);
 znew = matrix(0,300,0,300);
 fp = fopen("data1","r");
 for(i=0;i<256;i++){
 for(j=0;j<256;j++){
 fscanf(fp,"%f",&(z[i][j]));
 }
 }
 fclose(fp);
/* USER IS PROMPTED FOR PARAMETERS NEEDED TO CALCULATE HEIGHT
INFORMATION */
```

```
printf("\n Please input the scan size (in nm)");
scanf("%f",&scan_size);
printf("\n Please input the Z attenuation");
scanf("%f",&zatten);
printf("\n Please input the Z sensitivity");
scanf("%f",&zsens);
printf("\n Please input the Z maximum value");
scanf("%f",&zmax);
printf("\n Please input the Z scale value");
scanf("%f",&zheight);
printf("\n Please input the radius");
scanf("%f",&radius);
/* DATA IN z IS CONVERTED INTO NANOMETERS AND THE DATA IN znew IS
INITIALIZED
TO ZERO */

for(i=0;i<256;i++){
for(j=0;j<256;j++){
z[i][j] = (z[i][j]/65536.)*(zatten/65536.)*zsens*(2.*zmax/65536.)*zheight;
}
}
for(i=0;i<256;i++){
for(j=0;j<256;j++){
znew[i][j] = -2000.0;
}
}
/* WHAT FOLLOWS IS ALL THE COMBINATIONS OF POINTS i,j SUCH THAT
ALL THE DATA
```

```
IN z IS TRANSLATED INTO THE DECONVOLVED DATASET znew */
slope_x = slope_x_calc(z,scan_size,0,0);
slope_y = slope_y_calc(z,scan_size,0,0);
delta_x = del_x_calc(slope_x,slope_y,radius,scan_size);
delta_y = del_y_calc(slope_x,slope_y,radius,scan_size);
delta_z = del_z_calc(slope_x,slope_y,radius);
if(delta_x >=0 && delta_y >=0){
znew[delta_y][delta_x] = z[0][0] + delta_z;
}
slope_x = slope_x_calc(z,scan_size,0,1);
slope_y = slope_y_calc(z,scan_size,0,1);
delta_x = del_x_calc(slope_x,slope_y,radius,scan_size);
delta_y = del_y_calc(slope_x,slope_y,radius,scan_size);
delta_z = del_z_calc(slope_x,slope_y,radius);
if(delta_y >=0 && delta_x >-1.5){
znew[delta_y][1+delta_x] = z[0][1] + delta_z;
}
for(i=2;i<254;i++){
slope_x = slope_x_calc(z,scan_size,0,i);
slope_y = slope_y_calc(z,scan_size,0,i);
delta_x = del_x_calc(slope_x,slope_y,radius,scan_size);
delta_y = del_y_calc(slope_x,slope_y,radius,scan_size);
delta_z = del_z_calc(slope_x,slope_y,radius);
if(delta_y>=0.){
znew[delta_y][i+delta_x] = z[0][i] + delta_z;
}
}
slope_x = slope_x_calc(z,scan_size,0,254);
```

```
slope_y = slope_y_calc(z,scan_size,0,254);
delta_x = del_x_calc(slope_x,slope_y,radius,scan_size);
delta_y = del_y_calc(slope_x,slope_y,radius,scan_size);
delta_z = del_z_calc(slope_x,slope_y,radius);
if(delta_y >= 0.){
znew[delta_y][delta_x + 254] = z[0][254] + delta_z;
}
slope_x = slope_x_calc(z,scan_size,0,255);
slope_y = slope_y_calc(z,scan_size,0,255);
delta_x = del_x_calc(slope_x,slope_y,radius,scan_size);
delta_y = del_y_calc(slope_x,slope_y,radius,scan_size);
delta_z = del_z_calc(slope_x,slope_y,radius);
if(delta_y >= 0.){
znew[delta_y][delta_x + 255] = z[0][255] + delta_z;
}
slope_x = slope_x_calc(z,scan_size,1,0);
slope_y = slope_y_calc(z,scan_size,1,0);
delta_x = del_x_calc(slope_x,slope_y,radius,scan_size);
delta_y = del_y_calc(slope_x,slope_y,radius,scan_size);
delta_z = del_z_calc(slope_x,slope_y,radius);
if(delta_y > -1.1 && delta_x >= 0.){
znew[delta_y+1][delta_x] = z[1][0] + delta_z;
}
slope_x = slope_x_calc(z,scan_size,1,1);
slope_y = slope_y_calc(z,scan_size,1,1);
delta_x = del_x_calc(slope_x,slope_y,radius,scan_size);
delta_y = del_y_calc(slope_x,slope_y,radius,scan_size);
delta_z = del_z_calc(slope_x,slope_y,radius);
```

```
if(delta_y >= -1. && delta_x >= -1){
znew[delta_y+1][1+delta_x] = z[1][1] + delta_z;
}
for(i=2;i<254;i++){
slope_x = slope_x_calc(z,scan_size,1,i);
slope_y = slope_y_calc(z,scan_size,1,i);
delta_x = del_x_calc(slope_x,slope_y,radius,scan_size);
delta_y = del_y_calc(slope_x,slope_y,radius,scan_size);
delta_z = del_z_calc(slope_x,slope_y,radius);
if(delta_y >= -1 && delta_x >= -i){
znew[delta_y + 1][i+delta_x] = z[1][i] + delta_z;
}
}
slope_x = slope_x_calc(z,scan_size,1,254);
slope_y = slope_y_calc(z,scan_size,1,254);
delta_x = del_x_calc(slope_x,slope_y,radius,scan_size);
delta_y = del_y_calc(slope_x,slope_y,radius,scan_size);
delta_z = del_z_calc(slope_x,slope_y,radius);
if(delta_y >= -1 && delta_x <= 1){
znew[delta_y + 1][delta_x + 254] = z[1][254] + delta_z;
}
slope_x = slope_x_calc(z,scan_size,1,255);
slope_y = slope_y_calc(z,scan_size,1,255);
delta_x = del_x_calc(slope_x,slope_y,radius,scan_size);
delta_y = del_y_calc(slope_x,slope_y,radius,scan_size);
delta_z = del_z_calc(slope_x,slope_y,radius);
if(delta_y >= -1 && delta_x <= 0 ){
znew[delta_y + 1][delta_x + 255] = z[1][255] + delta_z;
```

```
}
for(i=2;i<254;i++){
slope_x = slope_x_calc(z,scan_size,i,0);
slope_y = slope_y_calc(z,scan_size,i,0);
delta_x = del_x_calc(slope_x,slope_y,radius,scan_size);
delta_y = del_y_calc(slope_x,slope_y,radius,scan_size);
delta_z = del_z_calc(slope_x,slope_y,radius);
if(delta_y >= -i && delta_x >= 0 && i+delta_y < 255){
znew[i+delta_y][delta_x] = z[i][0] + delta_z;
}
slope_x = slope_x_calc(z,scan_size,i,1);
slope_y = slope_y_calc(z,scan_size,i,1);
delta_x = del_x_calc(slope_x,slope_y,radius,scan_size);
delta_y = del_y_calc(slope_x,slope_y,radius,scan_size);
delta_z = del_z_calc(slope_x,slope_y,radius);
if(delta_y >= -i && delta_x >= -1 && i+delta_y < 256){
znew[i+delta_y][1+delta_x] = z[i][1] + delta_z;
}
for(j=2;j<254;j++){
slope_x = slope_x_calc(z,scan_size,i,j);
slope_y = slope_y_calc(z,scan_size,i,j);
delta_x = del_x_calc(slope_x,slope_y,radius,scan_size);
delta_y = del_y_calc(slope_x,slope_y,radius,scan_size);
delta_z = del_z_calc(slope_x,slope_y,radius);
if(i+delta_y >= 0 && i+delta_y <= 255 && delta_x >= -j){
znew[i+delta_y][j+delta_x] = z[i][j] + delta_z;
}
}
```

```
slope_x = slope_x_calc(z,scan_size,i,254);
slope_y = slope_y_calc(z,scan_size,i,254);
delta_x = del_x_calc(slope_x,slope_y,radius,scan_size);
delta_y = del_y_calc(slope_x,slope_y,radius,scan_size);
delta_z = del_z_calc(slope_x,slope_y,radius);
if(i+delta_y >= 0 && i+delta_y <= 255 && delta_x <= 1){
znew[i+delta_y][254+delta_x] = z[i][254] +delta_z;
}
slope_x = slope_x_calc(z,scan_size,i,255);
slope_y = slope_y_calc(z,scan_size,i,255);
delta_x = del_x_calc(slope_x,slope_y,radius,scan_size);
delta_y = del_y_calc(slope_x,slope_y,radius,scan_size);
delta_z = del_z_calc(slope_x,slope_y,radius);
if(i+delta_y >= 0 && i+delta_y <= 255 &&delta_x <=0 ){
znew[i+delta_y][255+delta_x] = z[i][255] +delta_z;
}
}
slope_x = slope_x_calc(z,scan_size,254,0);
slope_y = slope_y_calc(z,scan_size,254,0);
delta_x = del_x_calc(slope_x,slope_y,radius,scan_size);
delta_y = del_y_calc(slope_x,slope_y,radius,scan_size);
delta_z = del_z_calc(slope_x,slope_y,radius);
if(delta_y <= 1 && delta_x >= 0){
znew[254+delta_y][delta_x] = z[254][0] + delta_z;
}
slope_x = slope_x_calc(z,scan_size,254,1);
slope_y = slope_y_calc(z,scan_size,254,1);
delta_x = del_x_calc(slope_x,slope_y,radius,scan_size);
```

```
delta_y = del_y_calc(slope_x,slope_y,radius,scan_size);
delta_z = del_z_calc(slope_x,slope_y,radius);
if(delta_y <= 1 && delta_x >= -1 ){
znew[254+delta_y][1+delta_x] = z[254][1] + delta_z;
}
for(j=2;j<254;j++){
slope_x = slope_x_calc(z,scan_size,254,j);
slope_y = slope_y_calc(z,scan_size,254,j);
delta_x = del_x_calc(slope_x,slope_y,radius,scan_size);
delta_y = del_y_calc(slope_x,slope_y,radius,scan_size);
delta_z = del_z_calc(slope_x,slope_y,radius);
if(delta_y <= 1 && delta_x >= -j){
znew[254+delta_y][j+delta_x] = z[254][j] + delta_z;
}
}
slope_x = slope_x_calc(z,scan_size,254,254);
slope_y = slope_y_calc(z,scan_size,254,254);
delta_x = del_x_calc(slope_x,slope_y,radius,scan_size);
delta_y = del_y_calc(slope_x,slope_y,radius,scan_size);
delta_z = del_z_calc(slope_x,slope_y,radius);
if(delta_y <= 1 && delta_x <= 1){
znew[254+delta_y][254+delta_x] = z[254][254] + delta_z;
}
slope_x = slope_x_calc(z,scan_size,254,255);
slope_y = slope_y_calc(z,scan_size,254,255);
delta_x = del_x_calc(slope_x,slope_y,radius,scan_size);
delta_y = del_y_calc(slope_x,slope_y,radius,scan_size);
delta_z = del_z_calc(slope_x,slope_y,radius);
```

```
if(delta_y <= 1 && delta_x <=0){
znew[254+delta_y][255+delta_x] = z[254][255] + delta_z;
}
slope_x = slope_x_calc(z,scan_size,255,0);
slope_y = slope_y_calc(z,scan_size,255,0);
delta_x = del_x_calc(slope_x,slope_y,radius,scan_size);
delta_y = del_y_calc(slope_x,slope_y,radius,scan_size);
delta_z = del_z_calc(slope_x,slope_y,radius);
if(delta_y <= 0 && delta_x >= 0){
znew[255+delta_y][delta_x] = z[255][0] + delta_z;
}
slope_x = slope_x_calc(z,scan_size,255,1);
slope_y = slope_y_calc(z,scan_size,255,1);
delta_x = del_x_calc(slope_x,slope_y,radius,scan_size);
delta_y = del_y_calc(slope_x,slope_y,radius,scan_size);
delta_z = del_z_calc(slope_x,slope_y,radius);
if(delta_y <= 0 && delta_x >= -1){
znew[255+delta_y][1+delta_x] = z[255][1] + delta_z;
}
for(j=2;j<254;j++){
slope_x = slope_x_calc(z,scan_size,255,j);
slope_y = slope_y_calc(z,scan_size,255,j);
delta_x = del_x_calc(slope_x,slope_y,radius,scan_size);
delta_y = del_y_calc(slope_x,slope_y,radius,scan_size);
delta_z = del_z_calc(slope_x,slope_y,radius);
if(delta_y <= 0 && delta_x >= -j){
znew[255+delta_y][j+delta_x] = z[255][j] + delta_z;
}
```

```
}
slope_x = slope_x_calc(z,scan_size,255,254);
slope_y = slope_y_calc(z,scan_size,255,254);
delta_x = del_x_calc(slope_x,slope_y,radius,scan_size);
delta_y = del_y_calc(slope_x,slope_y,radius,scan_size);
delta_z = del_z_calc(slope_x,slope_y,radius);
if(delta_y <= 0 && delta_x <= 1){
znew[255+delta_y][254+delta_x] = z[255][254] + delta_z;
}
slope_x = slope_x_calc(z,scan_size,255,255);
slope_y = slope_y_calc(z,scan_size,255,255);
delta_x = del_x_calc(slope_x,slope_y,radius,scan_size);
delta_y = del_y_calc(slope_x,slope_y,radius,scan_size);
delta_z = del_z_calc(slope_x,slope_y,radius);
if(delta_y <=0 && delta_x <= 0){
znew[255+delta_y][255+delta_x] = z[255][255] + delta_z;
}
/* IF A POINT IN znew DOES NOT GET ASSIGNED A VALUE, AN INTERPOLATED VALUE
WILL BE ASSIGNED TO IT BY THE interpol ROUTINE */
interpol(znew);
/* FINALLY THE DATA IS CONVERTED FROM NANOMETERES TO DIMENSIONLESS VALUES */
for(i=0;i<256;i++){
for(j=0;j<256;j++){
znew[i][j] = (znew[i][j]/zatten)*(65536./zsens)*0.5*
(65536./zmax)*(65536/zheight);
}
```

```
}
/* DATA IS WRITTEN TO A DATAFILE CALLED decon.txt */
ofp = fopen("decon.txt","w");
for(i=0;i<256;i++){
for(k=0;k<32;k++){
for(j=0;j<8;j++){
fprintf(ofp,"%6.0f ",znew[i][8*k+j]);
}
fprintf(ofp,"\n");
}
}
fclose(ofp);
}
```

```
#include <stdio.h>
#include <math.h>
#include <stdlib.h>
#include "nrutil.h"
#include "convolution_calc.h"
int del_x_calc(float slope_x,float slope_y,float radius,float scan_size)
{
float delta_x;
int idelx;
delta_x = (slope_x/(sqrt(1.+slope_x*slope_x+slope_y*slope_y)))*radius;
delta_x = delta_x*(255./scan_size);
if(delta_x >0.){
idelx = 0.5 + delta_x;
}
```

```
 else {
 idelx = -0.5 + delta_x;
 }
 return idelx;
}
int del_y_calc(float slope_x,float slope_y,float radius,float scan_size)
{
 float delta_y;
 int idely;
 delta_y = (slope_y/(sqrt(1.+slope_x*slope_x+slope_y*slope_y)))*radius;
 delta_y = delta_y*(255./scan_size);
 if(delta_y > 0.){
 idely = 0.5 + delta_y;
 }
 else {
 idely = -0.5 + delta_y;
 }
 return idely;
}
float del_z_calc(float slope_x,float slope_y,float radius)
{
 float delta_z;

 delta_z = (-1.0/(sqrt(1.+slope_x*slope_x+slope_y*slope_y)))*radius;
 return delta_z;
}
float slope_x_calc(float **z,float scan_size,int i,int j)
{
```

```
float slope_x,coef;
coef = 255/(24.*scan_size);
if(j==0){
slope_x = coef*(-50*z[i][j]+96.*z[i][j+1]-72.*z[i][j+2]+32.*z[i][j+3]
-6.*z[i][j+4]);
}
if(j==1){
slope_x =coef*(-6.*z[i][j-1]-20.*z[i][j]+36.*z[i][j+1]-12.*z[i][j+2]
+2.*z[i][j+3]);
}
if(j==254){
slope_x = coef*(-2.*z[i][j-3]+12.*z[i][252]-36.*z[i][253]+20.*z[i][254]+6.*z[i][255]);
}
if(j==255){
slope_x = coef*(6.*z[i][251]-32.*z[i][252]+72.*z[i][253]-96.*z[i][254] +50.*z[i][255]);
}
if(j>1 && j<254){
slope_x = coef*(2.*z[i][j-2]-16.*z[i][j-1]+16.*z[i][j+1]-2.*z[i][j+2]);
}
return slope_x;
}
float slope_y_calc(float **z,float scan_size,int i, int j)
{
float slope_y,coef;
coef = 255./(24.*scan_size);
if(i==0){
slope_y = coef*(-50*z[0][j]+96.*z[1][j]-72.*z[2][j]+32.*z[3][j]
-6.*z[4][j]);
```

```
}
if(i==1){
slope_y = coef*(-6.*z[0][j]-20.*z[1][j]+36.*z[2][j]-12.*z[3][j]
+2.*z[4][j]);
}
if(i==254){
slope_y = coef*(-2.*z[251][j]+12.*z[252][j]-36.*z[253][j]+
20.*z[254][j]+6.*z[255][j]);
}
if(i==255){
slope_y = coef*(6.*z[251][j]-32.*z[252][j]+72.*z[253][j]-96.*z[254][j] +50.*z[255][j]);
}
if(i>1 && i<254){
slope_y = coef*(2.*z[i-2][j]-16.*z[i-1][j]+16.*z[i+1][j]
-2.*z[i+2][j]);
}
return slope_y;
}
void interpol(float **z)
{
int i,j,count=0;

for(i=2;i<254;i++){
for(j=2;j<254;j++){
if(z[i][j] == -2000.0){
z[i][j] = (z[i-2][j] + z[i][j-2]+z[i+2][j]+z[i][j+2]+3.*z[i][j-1]+3.*z[i][j+1]+3.*z[i+1][j]+3.*z[i-
1][j])/16.;
count++;
```

```
}
}
}
printf("\n Number of zeroes was: %d\n",count);
count = 0;
for(i=2;i<254;i++){
for(j=2;j<254;j++){
if(z[i][j] == -2000.) count++;
}
}
printf("\n The Number of zeroes after interpolation is: %d\n",count);
}
```

VITA

Matthew Joseph Klopfstein

Candidate for the Degree of

Master of Science

Thesis: SHAKEDOWN CHARACTERIZATION OF AN INSTRUMENT FOR NANOCUTTING AND NANOINDENTING

Major Field: Mechanical Engineering

Biographical:

Personal Data: Born in Columbus, Ohio, on July 18, 1968, the son of Joseph M. and Joyce N. Klopfstein

Education: Graduated from Worthington High School, Worthington, Ohio in June 1986; received Bachelor of Science degree in Mechanical Engineering from The Ohio State University, Columbus, Ohio in June 1991; received Master of Arts degree in Economics from The Ohio State University, Columbus, Ohio in August 1992. Completed the requirements for the Master of Science degree with a major in Mechanical Engineering at Oklahoma State University in December, 1997.